JCTC Journal of Chemical Theory and Computation

Article

Cite This: J. Chem. Theory Comput. 2018, 14, 1828−1840

pubs.acs.org/JCTC

Quasi-Diabatic Representation for Nonadiabatic Dynamics Propagation

Arkajit Mandal,[†,‡] Sharma SRKC Yamijala,[†,‡] and Pengfei Huo*[,†]

[†]Department of Chemistry, University of Rochester, 120 Trustee Road, Rochester, New York 14627, United States

Supporting Information

ABSTRACT: We develop a nonadiabatic dynamics propagation scheme that allows interfacing diabatic quantum dynamics methods with commonly used adiabatic electronic structure calculations. This scheme uses adiabatic states as the quasi-diabatic (QD) states during a short-time quantum dynamics propagation. At every dynamical propagation step, these QD states are updated based on a new set of adiabatic basis. Using the partial linearized density matrix (PLDM) path-integral method as one specific example for diabatic dynamics approaches, we demonstrate the accuracy of the QD scheme with a wide range of model nonadiabatic systems as well as the on-the-fly propagations with density functional tight-binding (DFTB) calculations. This study opens the possibility to combine accurate diabatic quantum dynamics methods with adiabatic electronic structure calculations for nonadiabatic dynamics propagations.

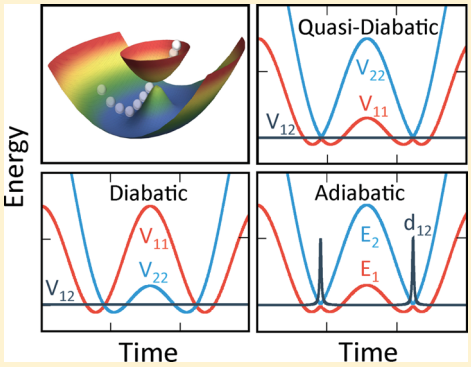

INTRODUCTION

One of the central challenges in modern theoretical chemistry is performing on-the-fly nonadiabatic dynamics simulations in an accurate and efficient fashion. This challenge boils down into two parts:[1] (i) electronic structure calculations that provide on-the-fly nuclear potential energy surfaces and electronic wave functions and (ii) dynamical propagations of the coupled electronic and nuclear motions. While extensive efforts have been focused on developing methods in each individual field, the incompatibility between electronic structure methods and quantum dynamics approaches remains to be addressed because they are usually developed in two different representations.

The majority of the electronic structure methods are formulated in the *adiabatic* representation, i.e., the eigenstates of the electronic Hamiltonian that parametrically depend on nuclear positions. The routinely available adiabatic electronic structure calculations have enabled on-the-fly dynamics propagations with approximate quantum dynamics approaches formulated in the same representation.[2−4] As a side note, here and throughout this paper, we refer to "quantum dynamics" approaches as those methods that incorporate electronic nonadiabatic transitions and/or nuclear quantum effects regardless of how they include these effects. These approximate quantum dynamics approaches such as widely used Ehrenfest dynamics or fewest switches surface hopping (FSSH),[3−5] however, are limited by their inherent mixed quantum-classical approximation,[1] which leads to the breakdown of detailed balance[6,7] or the creation of artificial electronic coherence.[4]

New quantum dynamics methods are developed to address the limitations and deficiencies of mixed quantum-classical approximations by treating electronic and nuclear dynamics on an equal classical footing[1,8−10] or rigorously preserving detailed balance.[11−13] Most of these recently emerged quantum dynamics approaches are developed in the *diabatic* representation,[9−12,14−16] i.e., a set of electronic states that do not explicitly depend upon nuclear positions. Under the diabatic representation, derivative couplings explicitly vanish,[17] providing a much simpler and convenient framework for quantum dynamics method development. In contrast to the adiabatic states, strict diabatic wave functions are neither uniquely defined nor routinely available, despite recent theoretical progress.[17−21] Thus, the typical strategy for applying these new methods to "real" molecular systems is to reformulate them in the adiabatic representation,[8,22−24] which usually requires tedious theoretical efforts. Moreover, the adiabatic version of these methods are computationally inconvenient due to the presence of the first- and second-order derivative couplings,[22] which could potentially lead to numerical instabilities during dynamical propagations.

The discrepancy between the accurate and convenient dynamics approaches in the *diabatic* representation and the routinely available electronic structure calculations in the *adiabatic* representation has significantly hampered our ability to accurately and efficiently perform on-the-fly quantum dynamics simulations.

To address this challenge, here we apply a quasi-diabatic (QD) scheme that allows combining *diabatic* dynamics approaches with *adiabatic* electronic structure calculations for direct quantum dynamics propagation. Within this scheme, the adiabatic states from routine electronic structure calculations

Received: November 21, 2017
Published: February 28, 2018

DOI: 10.1021/acs.jctc.7b01178
J. Chem. Theory Comput. 2018, 14, 1828−1840

are used as quasi-diabatic states during a short-time propagation. Between two consecutive short-time propagations, the representation is transformed from the old to the new QD states. We should note that the QD scheme has been previously used to provide a numerically stable integration of the time-dependent Schrödinger equation (TDSE).[25−32] Here, we expand the scope and the applicability of this scheme by using it as a general framework to interface *diabatic* quantum dynamics methods and *adiabatic* electronic structure calculations.

In this paper, we demonstrate the accuracy of the QD propagation scheme by using the recently developed partial linearized density matrix (PLDM) path-integral method[10,33] as one example of the diabatic dynamics methods. Quantum dynamics simulations of the model systems as well as the on-the-fly calculations suggest an excellent agreement between the QD propagation scheme and the diabatic PLDM method or the numerical solution of TDSE. The QD scheme provides a general and seamless framework to combine accurate diabatic quantum dynamics methods with commonly used adiabatic electronic structure calculations for nonadiabatic quantum dynamics propagations.

THEORY AND METHOD

Adiabatic and Diabatic Representations. We begin with a brief introduction of the adiabatic and the diabatic representations. The total Hamiltonian for a given molecular system can be expressed as a sum of the nuclear kinetic energy operator $\hat{T}$ and the electronic Hamiltonian operator $\hat{V}(\hat{\mathbf{r}}, \hat{\mathbf{R}})$ as follows

$$\hat{H} = \hat{T} + \hat{V}(\hat{\mathbf{r}}, \hat{\mathbf{R}}) \tag{1}$$

Here, $\hat{\mathbf{r}}$ represents the coordinate operator of the electronic degrees of freedom (DOF), and $\hat{\mathbf{R}}$ represents the coordinate operator of the nuclear DOF.

Based on the Born−Oppenheimer approximation, it is convenient to solve the eigenequation of the electronic Hamiltonian operator at a given *value* of the nuclear coordinate operator

$$\hat{V}(\hat{\mathbf{r}};\ \mathbf{R})|\Phi_i(\mathbf{r};\ \mathbf{R})\rangle = E_i(\mathbf{R})|\Phi_i(\mathbf{r};\ \mathbf{R})\rangle \tag{2}$$

Here, $|\Phi_i(\mathbf{r};\ \mathbf{R})\rangle$ is the *adiabatic* state, i.e., the eigenstate of $\hat{V}(\hat{\mathbf{r}};\ \mathbf{R})$. A majority of the commonly used electronic structure methods are based on solving the above equation, providing eigenenergies and eigenfunctions under this representation.

In the adiabatic representation, the total Hamiltonian in eq 1 is expressed as the following "vibronic Hamiltonian" operator (with $\hbar = 1$)

$$\hat{H} = \frac{\hat{\mathbf{P}}^2}{2M} + \sum_i E_i(\mathbf{R})|\Phi_i(\mathbf{r};\ \mathbf{R})\rangle\langle\Phi_i(\mathbf{r};\ \mathbf{R})| - \sum_{ij}\left[i\frac{\hat{\mathbf{P}}}{M}\mathbf{d}_{ij}(\mathbf{R}) + \frac{D_{ij}(\mathbf{R})}{2M}\right]|\Phi_i(\mathbf{r};\ \mathbf{R})\rangle\langle\Phi_j(\mathbf{r};\ \mathbf{R})| \tag{3}$$

where $\mathbf{d}_{ij}(\mathbf{R}) = \langle\Phi_i(\mathbf{r};\ \mathbf{R})|\nabla|\Phi_j(\mathbf{r};\ \mathbf{R})\rangle$ is the derivative coupling vector, $D_{ij}(\mathbf{R}) = \langle\Phi_i(\mathbf{r};\ \mathbf{R})|\nabla^2|\Phi_j(\mathbf{r};\ \mathbf{R})\rangle$ is the second-derivative coupling, and the diagonal terms $D_{ii}(\mathbf{R})$ are usually referred as the Born−Oppenheimer (BO) corrections.

One can see that despite the compact expression of $\hat{V}(\hat{\mathbf{r}};\ \mathbf{R})$ under its own eigenstates, the adiabatic states indeed make the total Hamiltonian complicated, due to the fact that they are not the eigenfunctions of the nuclear kinetic energy operator. Thus, the adiabatic representation is not convenient for solving quantum dynamics problems governed by the total Hamiltonian (eq 3), although it is well-suited for electronic structure calculations (eq 2).

Alternatively, one can use the *diabatic* basis which is independent of nuclear coordinates and, thus, make $\mathbf{d}_{ij}(\mathbf{R})$ and $D_{ij}(\mathbf{R})$ vanish. It turns out that there are infinite ways to choose the diabatic basis. One trivial way to construct diabatic states is to simply use the adiabatic basis $\{|\Phi_i(\mathbf{r};\ \mathbf{R_0})\rangle\}$ at a reference nuclear geometry $\mathbf{R_0}$. Then, the total Hamiltonian operator becomes

$$\hat{H} = \frac{\hat{\mathbf{P}}^2}{2M} + \sum_{i,j} V_{ij}(\mathbf{R})|\Phi_i(\mathbf{r};\ \mathbf{R_0})\rangle\langle\Phi_j(\mathbf{r};\ \mathbf{R_0})| \tag{4}$$

with $V_{ij}(\mathbf{R}) = \langle\Phi_i(\mathbf{r};\ \mathbf{R_0})|\hat{V}(\hat{\mathbf{r}};\ \mathbf{R})|\Phi_j(\mathbf{r};\ \mathbf{R_0})\rangle$. The above diabatic basis are usually called the "crude adiabatic" basis (CAB).[34−36] In this paper, we refer to CAB as the quasi-diabatic (QD) basis.

Compared to the adiabatic representation, the advantage of the QD basis is that all of the derivative couplings vanish, and the nonadiabatic transitions are only induced by the diabatic coupling elements $V_{ij}(\mathbf{R})$. As a consequence, the total Hamiltonian operator and the corresponding quantum dynamics propagation adapt a simpler form in the QD representation. However, because that the electronic wave function changes rapidly with the motion of the nuclei, the QD basis is convenient only when the nuclear geometry $\mathbf{R}$ is close to the reference geometry $\mathbf{R_0}$.

Quasi-Diabatic (QD) Propagation Scheme. Now, we provide a detailed description of the QD scheme that can resolve the incompatibility between the diabatic dynamics approaches and the adiabatic electronic structure methods.

Consider a short-time propagation of the nuclear DOF during $t \in [t_1, t_2]$, where the nuclear positions evolve from $\mathbf{R}(t_1)$ to $\mathbf{R}(t_2)$ and the corresponding adiabatic states are $\{|\Phi_i(\mathbf{r};\ \mathbf{R}(t_1))\rangle\}$ and $\{|\Phi_j(\mathbf{r};\ \mathbf{R}(t_2))\rangle\}$. The key idea of the QD scheme is to use the nuclear geometry at time t_1 as the reference geometry, $\mathbf{R_0} \equiv \mathbf{R}(t_1)$, and use the adiabatic basis $\{|\Phi_i(\mathbf{r};\ \mathbf{R}(t_1))\rangle\}$ as the *quasi-diabatic* basis during this short-time quantum dynamics propagation, such that

$$|\Phi_i(\mathbf{r};\ \mathbf{R_0})\rangle \equiv |\Phi_i(\mathbf{r};\ \mathbf{R}(t_1))\rangle, \text{ for } t \in [t_1, t_2] \tag{5}$$

With the above QD basis, the derivative couplings vanish in a trivial way, and $\hat{V}(\hat{\mathbf{r}};\ \mathbf{R})$ has off-diagonal elements. During the next short-time propagation segment $t \in [t_2, t_3]$, we use a new reference geometry $\mathbf{R}_0' \equiv \mathbf{R}(t_2)$ and *quasi-diabatic* basis $|\Phi_k'(\mathbf{r};\mathbf{R}_0')\rangle \equiv |\Phi_k(\mathbf{r};\ \mathbf{R}(t_2))\rangle$. With the nuclear geometry close to the reference geometry in each step, the QD representation remains to be a convenient and compact basis in each short-term propagation segment. In addition, because of the diabatic nature of the QD basis, one can use any diabatic-based approach to propagate the quantum dynamics. These approaches usually require diabatic energies, electronic couplings, and nuclear gradients. Between $[t_1, t_2]$ propagation and $[t_2, t_3]$ propagation segments, all of these quantities will be transformed from $\{|\Phi_i(\mathbf{r};\ \mathbf{R_0})\rangle\}$ basis to $\{|\Phi'_k(\mathbf{r};\mathbf{R}_0')\rangle\}$ basis.

Next, we briefly summarize how to obtain these electronic couplings and nuclear gradients within the QD scheme. During the $t \in [t_1, t_2]$ short-time propagation, the electronic Hamiltonian operator $\hat{V}(\hat{\mathbf{r}};\ \mathbf{R}(t))$ is expressed as

$$V_{ij}(\mathbf{R}(t)) = \langle\Phi_i(\mathbf{r};\ \mathbf{R_0})|\hat{V}(\hat{\mathbf{r}};\ \mathbf{R}(t))|\Phi_j(\mathbf{r};\ \mathbf{R_0})\rangle \tag{6}$$

DOI: 10.1021/acs.jctc.7b01178
J. Chem. Theory Comput. 2018, 14, 1828−1840

In practical on-the-fly calculations, the above quantity can be obtained by a linear interpolation between $V_{ij}(\mathbf{R}(t_1))$ and $V_{ij}(\mathbf{R}(t_2))$ as follows[25]

$$V_{ij}(\mathbf{R}(t)) = V_{ij}(\mathbf{R}(t_1)) + \frac{(t - t_1)}{(t_2 - t_1)}[V_{ij}(\mathbf{R}(t_2)) - V_{ij}(\mathbf{R}(t_1))] \tag{7}$$

Here, the matrix elements $V_{ij}(\mathbf{R}(t_1)) = \langle \Phi_i\ (\mathbf{r};\ \mathbf{R_0})|\hat{V}(\hat{\mathbf{r}};\mathbf{R}(t_1))|\Phi_j\ (\mathbf{r};\ \mathbf{R_0})\rangle = E_j(\mathbf{R}(t_1))\ \delta_{ij}$ and the matrix elements $V_{ij}(\mathbf{R}(t_2))$ can be easily computed as follows

$$V_{ij}(\mathbf{R}(t_2)) = \sum_{kl} b_{ik} b_{jl}^{\dagger} \langle \Phi_k(\mathbf{r};\ \mathbf{R}(t_2))|\hat{V}(\hat{\mathbf{r}};\ \mathbf{R}(t_2))|\Phi_l(\mathbf{r};\ \mathbf{R}(t_2))\rangle \tag{8}$$

where $\langle \Phi_k(\mathbf{r};\ \mathbf{R}(t_2))|\hat{V}\ (\hat{\mathbf{r}};\ \mathbf{R}(t_2))|\Phi_l(\mathbf{r};\ \mathbf{R}(t_2))\rangle = E_l(\mathbf{R}(t_2))\ \delta_{kl}$, $b_{ik} = \langle \Phi_i(\mathbf{r};\ \mathbf{R_0})|\Phi_k(\mathbf{r};\ \mathbf{R}(t_2))\rangle$ and $b^{\dagger}_{jl} = \langle \Phi_l(\mathbf{r};\ \mathbf{R}(t_2))|\Phi_j(\mathbf{r};\ \mathbf{R_0})\rangle$. The above linear interpolation scheme can be further improved in the future work; one potential choice is the recently developed norm-preserving interpolation scheme.[37,38]

Similarly, the nuclear gradients on electronic Hamiltonian matrix elements $\nabla V_{ij}(\mathbf{R}(t_2)) \equiv \partial V_{ij}(\mathbf{R}(t_2))/\partial \mathbf{R}$ are evaluated as

$$\begin{aligned} \nabla V_{ij}(\mathbf{R}(t_2)) &= \nabla \langle \Phi_i(\mathbf{r};\ \mathbf{R}_0)|\hat{V}(\hat{\mathbf{r}};\ \mathbf{R}(t_2))|\Phi_j(\mathbf{r};\ \mathbf{R}_0)\rangle \\ &= \langle \Phi_i(\mathbf{r};\ \mathbf{R}_0)|\nabla \hat{V}(\hat{\mathbf{r}};\ \mathbf{R}(t_2))|\Phi_j(\mathbf{r};\ \mathbf{R}_0)\rangle \\ &= \sum_{kl} b_{ik} \langle \Phi_k(\mathbf{r};\ \mathbf{R}(t_2))|\nabla \hat{V}(\hat{\mathbf{r}};\ \mathbf{R}(t_2))|\Phi_l(\mathbf{r};\ \mathbf{R}(t_2))\rangle b_{jl}^{\dagger} \end{aligned} \tag{9}$$

Here, we have used the fact that $\{|\Phi_i(\mathbf{r};\ \mathbf{R_0})\rangle\}$ is a *diabatic* basis during the $[t_1,\ t_2]$ propagation, which allows moving the gradient operator to bypass $\langle \Phi_i(\mathbf{r};\ \mathbf{R_0})|$. In addition, we have inserted the resolution of identity

$$\sum_k |\Phi_k(\mathbf{r};\ \mathbf{R}(t_2))\rangle\langle \Phi_k(\mathbf{r};\ \mathbf{R}(t_2))| = 1$$

where we explicitly assume that this basis at nuclear position $\mathbf{R}(t_2)$ is complete. Note that $\{|\Phi_k(\mathbf{r};\mathbf{R}(t_2))\rangle\}$ is an *adiabatic* basis during this propagation step, due to the fact that $\mathbf{R}(t_2)$ is a changing geometry during the $[t_1,\ t_2]$ propagation rather than a fixed reference geometry. Since $\{|\Phi_k(\mathbf{r};\mathbf{R}(t_2))\rangle\}$ are the adiabatic states during this propagation step, we can directly obtain $\langle \Phi_k(\mathbf{r};\ \mathbf{R}(t_2))|\nabla \hat{V}(\hat{\mathbf{r}};\ \mathbf{R}(t_2))|\Phi_l(\mathbf{r};\ \mathbf{R}(t_2))\rangle$ from standard electronic structure calculations.

Further, we emphasize that in the QD propagation scheme, only $\langle \Phi_k(\mathbf{r};\ \mathbf{R})|\nabla \hat{V}(\hat{\mathbf{r}};\ \mathbf{R})|\Phi_l(\mathbf{r};\ \mathbf{R})\rangle$ is needed. The derivative couplings

$$\mathbf{d}_{kl}(\mathbf{R}) = \frac{\langle \Phi_k(\mathbf{r};\ \mathbf{R})|\nabla \hat{V}(\hat{\mathbf{r}};\ \mathbf{R})|\Phi_l(\mathbf{r};\ \mathbf{R})\rangle}{E_l(\mathbf{R}) - E_k(\mathbf{R})} \tag{10}$$

on the other hand, are not explicitly required. One should note that $\mathbf{d}_{kl}(\mathbf{R})$ can become singular due to the degeneracy of eigenvalues, i.e., $E_l(\mathbf{R}) - E_k(\mathbf{R}) = 0$, even when $\langle \Phi_k(\mathbf{r};\ \mathbf{R})|\nabla \hat{V}(\hat{\mathbf{r}};\ \mathbf{R})|\Phi_l(\mathbf{r};\ \mathbf{R})\rangle$ is finite. Thus, the method that directly requires derivative couplings might suffer from numerical instabilities, whereas the QD propagation scheme will not.

In order to provide a detailed picture of the adiabatic, diabatic, and quasi-diabatic basis, we consider a simple model system. The model contains two electronic states and one nuclear coordinate, with the potential operator $\hat{V}(R) = 0.5\omega^2 R^2 + \Delta\hat{\sigma}_x + cR\hat{\sigma}_z$, where the electron−phonon coupling is $c = 1$, the phonon vibrational frequency is $\omega = 1$, and the electronic coupling is $\Delta = 0.1$. This potential is illustrated in the inset of Figure 1a. To simplify our discussion, we initiate the nuclear trajectory on the diabatic state 1 (red surface in the inset of Figure 1a) and constrain the motion of the trajectory on that surface.

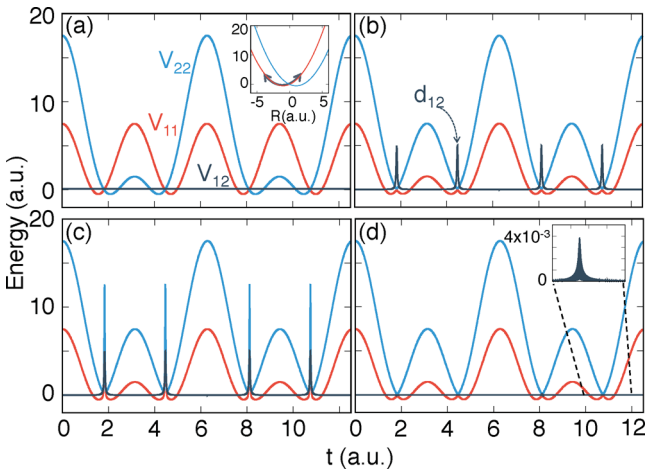

Figure 1. Time-dependent potentials and couplings for a model system in (a) diabatic representation (inset: diabatic potential), (b) adiabatic representation, (c) adiabatic representation with Born−Oppenheimer corrections, and (d) quasi-diabatic representation (inset: time-dependent electronic coupling).

Figure 1a presents the matrix elements of the electronic Hamiltonian in the diabatic representation, with diabatic potential energy surfaces $V_{11}(R(t))$ and $V_{22}(R(t))$, as well as a constant diabatic electronic coupling $V_{12}(R(t)) = \Delta = 0.1$. By the model construction, the matrix elements of $\hat{V}$ under the diabatic representation exhibit smooth time evolution.

Figure 1b presents $\hat{V}(R)$ in the adiabatic representation. At the avoided crossing region where the adiabatic wave functions rapidly change their characters, the derivative coupling vector $d_{12}(R) = \langle \Phi_1(R)|\nabla|\Phi_2(R)\rangle$ starts to exhibit large peaks. These rapid changes of $d_{12}(R)$ cause numerical challenges for direct integration of TDSE (see eq 22 in Appendix A).

The situation becomes more complicated when considering Born−Oppenheimer (BO) corrections $\langle \Phi_i(R)|\nabla^2|\Phi_i(R)\rangle/2M$ for the adiabatic surfaces. As depicted in Figure 1c, even the potentials $E_i(R) + \langle \Phi_i(R)|\nabla^2|\Phi_i(R)\rangle/2M$ are highly peaked due to these BO corrections. Simply ignoring the BO corrections might cause additional errors in approximate quantum dynamics approaches.[22,39]

Figure 1d presents the $\hat{V}(R)$ in the quasi-diabatic representation. Here, the off-diagonal electronic couplings have small values due to the varying QD basis along the propagation, as illustrated in the in the inset of this panel. These couplings decrease to zero under the limit that $t_2 - t_1 \rightarrow 0$, and the nonadiabatic transitions are purely induced by the overlap between two consecutive QD bases $\langle \Phi_j(\mathbf{r};\ \mathbf{R}(t_2))|\Phi_i(\mathbf{r};\ \mathbf{R}(t_1))\rangle$.

The QD representation provides several unique advantages over the strict diabatic or adiabatic representation for quantum dynamics propagations. On one hand, the QD basis are constructed from the crude adiabatic basis, which can be easily obtained from any widely used electronic structure calculations. On the other hand, the diabatic nature of the QD basis makes derivative couplings explicitly vanish and allows using any diabatic dynamics approaches to perform on-the-fly propagation.

DOI: 10.1021/acs.jctc.7b01178
J. Chem. Theory Comput. 2018, 14, 1828−1840

Further, the QD representation ensures a stable propagation of the electronic quantum dynamics compared to directly solving TDSE in the adiabatic representation. This is due to the fact that directly solving TDSE requires the nonadiabatic coupling $\langle \Phi_j(\mathbf{r};\ \mathbf{R}(t))|\frac{\partial}{\partial t}\Phi_i(\mathbf{r};\ \mathbf{R}(t))\rangle = \mathbf{d}_{ji}(\mathbf{R})\dot{\mathbf{R}}$, which might exhibit highly peaked values and cause large numerical errors[37,38] when using the linear interpolation scheme.[40] A recently developed norm-preserving interpolation scheme[37,38] addresses this issue by providing accurate values of nonadiabatic couplings, resulting in a much more stable procedure for integrating TDSE. The QD scheme, on the other hand, explicitly alleviates this difficulty by using the well-behaved transformation matrix elements $\langle \Phi_j(\mathbf{r};\ \mathbf{R}(t_1))|\Phi_i(\mathbf{r};\ \mathbf{R}(t_2))\rangle$ instead of $\langle \Phi_j(\mathbf{r};\ \mathbf{R}(t))|\frac{\partial}{\partial t}\Phi_i(\mathbf{r};\ \mathbf{R}(t))\rangle$. The numerical advantage of the QD scheme compared to the adiabatic propagation scheme (i.e., solving the equation of motion for the adiabatic mapping Hamiltonian in Appendix B) is thus most significant when the derivative couplings are highly peaked. For example, with the model system presented in Figure 1, our numerical results suggest that one can use a relatively large time step in the QD propagation scheme, whereas in the adiabatic mapping propagation scheme, a time step that is at least 10 times smaller is required to integrate the equation of motion in order to obtain accurate results.

The essential idea of QD propagation can be dated back to the Magnus expansion[41] for solving TDSE. Similar schemes have been developed[25,30,32] to provide a stable integration of TDSE, with one particular scheme[25] provided in Appendix A. However, we should emphasize that these previous applications (which are mainly FSSH calculations) only use a QD scheme to evolve the quantum amplitudes, whereas the nuclei are still propagated on the *adiabatic* surfaces[30,32] or with forces expressed in the *adiabatic* representation.[42] In this paper, we expand the scope and the applicability of the QD scheme by using it as a general framework to interface *diabatic* quantum dynamics methods and *adiabatic* electronic structure calculations. In addition, we propagate both electronic and nuclear DOF in the same QD representation.

Finally, the QD scheme allows using recently developed diabatic quantum dynamics methods to perform on-the-fly propagations and avoids additional efforts to reformulate these approaches in the adiabatic representation. These new dynamics methods include, but are not limited to, the symmetrical quasi-classical (SQC) approach,[9,43−46] quantum-classical Liouville equation (QCLE) dynamics,[14,47−50] quantum-classical path integral (QCPI) approach,[51−54] and nonadiabatic ring polymer molecular dynamics (NRPMD) approach.[15] To illustrate this idea, we use the partial linearized density matrix (PLDM) path-integral approach[10,33] as one specific example to perform quantum dynamics propagation with the QD scheme.

Partial Linearized Density Matrix (PLDM) Path-Integral Method. We provide a brief outline of the PLDM approach.[10,33] We begin with expressing the total Hamiltonian in terms of nuclear kinetic energy and potential energy operators

$$\hat{H} = \hat{T} + V_0(\hat{\mathbf{R}}) + \sum_{\alpha,\beta} V_{\alpha\beta}(\hat{\mathbf{R}})|\alpha\rangle\langle\beta| \tag{11}$$

where $\{|\alpha\rangle, |\beta\rangle\}$ are the strict diabatic basis, $V_{\alpha\beta}(\hat{\mathbf{R}})$ is the state-dependent potential, and $V_0(\hat{\mathbf{R}})$ is the state-independent potential. By using the mapping representation of Meyer−Miller−Stock−Thoss[55−57] to transform the discrete electronic states into continuous variables, we have $|\alpha\rangle\langle\beta| \rightarrow \hat{a}_\alpha^\dagger \hat{a}_\beta$, where $\hat{a}_\alpha^\dagger = \left(\hat{q}_\alpha - i\hat{p}_\alpha\right)/\sqrt{2}$. With this transformation, the nonadiabatic transitions between electronic states are exactly mapped onto the classical motion of fictitious harmonic oscillators. Thus, MMST mapping Hamiltonian provides a consistent classical footing for both electronic and nuclear DOFs.

Applying a partial linearization approximation[10] only to the nuclear DOF and keeping the explicit propagation of the electronic mapping DOF for both forward and backward paths, we arrive at the PLDM expression for computing reduced density matrix[10,33]

$$\begin{aligned}\rho_{\alpha\beta}(t) &= \mathrm{Tr}_{\mathbf{R}}\left[\hat{\rho}(0)e^{i\hat{H}t/\hbar}|\alpha\rangle\langle\beta|e^{-i\hat{H}t/\hbar}\right] \\ &\approx \sum_{\gamma\mu}\int d\mathbf{R}\frac{d\mathbf{P}}{2\pi\hbar}d\mathbf{q}d\mathbf{p}d\mathbf{q}'d\mathbf{p}' G_0 G_0'[\hat{\rho}(0)_{\gamma\mu}^{\mathrm{W}}]T_{\gamma\alpha}T'_{\beta\mu}\end{aligned} \tag{12}$$

where

$$T_{\gamma\alpha} = \frac{1}{2}(q_\alpha(t) + ip_\alpha(t))(q_\gamma(0) - ip_\gamma(0))$$

and

$$T'_{\beta\mu} = \frac{1}{2}(q_\mu(0) + ip_\mu(0))(q_\beta(t) - ip_\beta(t))$$

are the electronic transition amplitudes, and $[\hat{\rho}(0)_{\gamma\mu}^{\mathrm{W}}]$ is the partial Wigner transform (with respect to the nuclear DOF) of the $\gamma\mu^{\mathrm{th}}$ matrix element of the initial density operators $\hat{\rho}(0)$. The initial distribution of electronic DOF is sampled from the coherent state (Husimi) distribution, with $G_0(\mathbf{q},\mathbf{p}) = e^{-1/2\sum_\nu(q_\nu^2+p_\nu^2)}$ and $G_0'(\mathbf{q}',\mathbf{p}') = e^{-1/2\sum_\zeta(q_\zeta'^2+p_\zeta'^2)}$.

Classical trajectories are used to evaluate the approximate time-dependent reduced density matrix in eq 12. The forward mapping variables are evolved based on the Hamilton's equations of motion[10,33]

$$\dot{q}_\alpha = \partial h_{\mathrm{m}}/\partial p_\alpha; \quad \dot{p}_\alpha = -\partial h_{\mathrm{m}}/\partial q_\alpha \tag{13}$$

where h_{m} is the *classical* mapping Hamiltonian[10,58] with the following expression

$$h_{\mathrm{m}}(\mathbf{R},\mathbf{p},\mathbf{q}) = \frac{1}{2}\sum_{\alpha\beta} V_{\alpha\beta}(R)(p_\alpha p_\beta + q_\alpha q_\beta) \tag{14}$$

The backward mapping variables are propagated with the similar equations of motion governed by $h_{\mathrm{m}}(\mathbf{R},\mathbf{p}',\mathbf{q}')$. The nuclei are propagated with the force[10]

$$\mathbf{F} = \mathbf{F}_0 + \mathbf{F}_{\mathrm{e}} \tag{15}$$

where $\mathbf{F}_0 = -\nabla V_0(\mathbf{R})$ is the state-independent force and $\mathbf{F}_{\mathrm{e}}$ is the state-dependent force with the following expression[10]

$$\mathbf{F}_{\mathrm{e}} = -\frac{1}{4}\sum_{\alpha\beta}\nabla V_{\alpha\beta}(R)\left[p_\alpha p_\beta + q_\alpha q_\beta + p'_\alpha p'_\beta + q'_\alpha q'_\beta\right] \tag{16}$$

PLDM uses consistent dynamical footing for both electronic and nuclear DOFs and, thus, accurately describes their coupled motion. In contrast, widely used mixed quantum-classical methods such as Ehrenfest or FSSH[1,5] treat quantum and

DOI: 10.1021/acs.jctc.7b01178
J. Chem. Theory Comput. 2018, 14, 1828−1840

classical DOFs on different footings, which causes the breakdown of detailed balance[6,7] or creating the artificial electronic coherence.[4,5] In addition, compared to the closely related methods that fully linearize both mapping and nuclear DOFs,[50,59,60] PLDM retains full dynamical propagation along both forward and backward paths for the mapping DOF, thus achieving a more accurate description of the electronic dynamics.[10,14,61] PLDM has been successfully applied to simulate a broad range of nonadiabatic processes, including excitation energy transfer dynamics,[33,62] electron transfer reactions,[61] and singlet fission quantum dynamics,[63] as well as nonlinear optical spectroscopy calculations.[64]

QD-PLDM Propagation. Combining the QD scheme and the diabatic PLDM approach described in the previous sections, we formulate the following algorithm for quantum dynamics propagation:

(1) Sample the initial conditions of the nuclear DOF $\mathbf{R}(t_1)$ and $\mathbf{P}\left(t_1 + \frac{\Delta t}{2}\right)$ based on the Wigner distribution $[\hat{\rho}(0)^{\mathrm{W}}_{\gamma\mu}]$, where $\Delta t = t_2 - t_1$, and sample the mapping variables based on the Husimi distribution $G_0(\mathbf{q},\mathbf{p})$ and $G'_0(\mathbf{q}',\mathbf{p}')$.

(2) Perform electronic structure calculations at t_1 to obtain the QD basis $|\Phi_i(\mathbf{r};\mathbf{R_0})\rangle \equiv |\Phi_i(\mathbf{r};\mathbf{R}(t_1))\rangle$.

(3) Propagate nuclear positions as

$$\mathbf{R}(t_2) = \mathbf{R}(t_1) + \mathbf{P}\left(t_1 + \frac{\Delta t}{2}\right)\Delta t/M$$

perform electronic structure calculations at $\mathbf{R}(t_2)$ to obtain the adiabatic basis $\{|\Phi_k(\mathbf{r};\mathbf{R}(t_2))\rangle\}$.

(4) Compute the electronic Hamiltonian elements $V_{ij}(\mathbf{R}(t))$ based on eq 7 for $t \in [t_1, t_2]$, as well as the nuclear gradients $\nabla V_{ij}(\mathbf{R}(t_2))$ based on eq 9.

(5) Propagate the forward and backward mapping variables $\{\mathbf{q},\mathbf{p}\}$ and $\{\mathbf{q}',\mathbf{p}'\}$ by solving Hamilton's equations of motion in eq 13, with the electronic elements $V_{ij}(\mathbf{R}(t))$ computed from step **4**; propagate the nuclear momenta as

$$\mathbf{P}\left(t_2 + \frac{\Delta t}{2}\right) = \mathbf{P}\left(t_1 + \frac{\Delta t}{2}\right) + \mathbf{F}(\mathbf{R}(t_2))\Delta t/M$$

with the force computed at nuclear position $\mathbf{R}(t_2)$ based on eq 15.

(6) Transform the mapping variables into the new QD basis $|\Phi'_k(\mathbf{r};\mathbf{R'_0})\rangle \equiv |\Phi_k(\mathbf{r};\mathbf{R}(t_2))\rangle$ for the $[t_2, t_3]$ propagation step, with the following expressions: $\sum_i q_i \langle\Phi_i(\mathbf{r};\mathbf{R}(t_1))|\Phi_k(\mathbf{r};\mathbf{R}(t_2))\rangle \to q_k$ and $\sum_i p_i \langle\Phi_i(\mathbf{r};\mathbf{R}(t_1))|\Phi_k(\mathbf{r};\mathbf{R}(t_2))\rangle \to p_k$.

(7) Repeat steps **3**–**6**.

Here, we would like to justify two technical choices in steps **5** and **6** of the above algorithm.

First, we transform the mapping variables between two bases, with the expression provided in step **6**. This expression is valid due to the fact that the relations between two QD bases are $|\Phi_k(\mathbf{r};\mathbf{R}(t_2))\rangle = \sum_i \langle\Phi_i(\mathbf{r};\mathbf{R}(t_1))|\Phi_k(\mathbf{r};\mathbf{R}(t_2))\rangle|\Phi_i(\mathbf{r};\mathbf{R}(t_1))\rangle$. Since the mapping relation between the physical state and the singly excited oscillator state is

$$|\Phi_k(\mathbf{r};\mathbf{R}(t_2))\rangle = a_k^\dagger|0\rangle = \frac{1}{\sqrt{2}}(\hat{q}_k + i\hat{p}_k)|0\rangle$$

the relations for the mapping variables associated with two bases are

$$\begin{aligned}|\Phi_k(\mathbf{r};\mathbf{R}(t_2))\rangle &= \frac{1}{\sqrt{2}}(\hat{q}_k + i\hat{p}_k)|0\rangle \\ &= \sum_i \langle\Phi_i(\mathbf{r};\mathbf{R}(t_1))|\Phi_k(\mathbf{r};\mathbf{R}(t_2))\rangle \\ &\times \frac{1}{\sqrt{2}}(\hat{q}_i + i\hat{p}_i)|0\rangle\end{aligned} \tag{17}$$

For molecular systems, one can always find a suitable choice of the basis set to make $\langle\Phi_i(\mathbf{r};\mathbf{R}(t_1))|\Phi_k(\mathbf{r};\mathbf{R}(t_2))\rangle$ real. Thus, it is guaranteed that the mapping variables are transformed with the same relations as the bases.

Second, the nuclear QD-PLDM force used in step **5** has the same form of the PLDM force in the strict diabatic basis $\{|\alpha\rangle\}$. This is valid based on the following analysis. Consider to expand the strict diabatic basis as the linear combination of QD basis, with $|\alpha\rangle = \sum_i|\Phi_i(\mathbf{r};\mathbf{R_0})\rangle\langle\Phi_i(\mathbf{r};\mathbf{R_0})|\alpha\rangle = \sum_\alpha C_{i\alpha}|\Phi_i(\mathbf{r};\mathbf{R_0})\rangle$. This implies that $q_\alpha = \sum_i C_{i\alpha}q_i$ and $p_\alpha = \sum_i C_{i\alpha}p_i$. Plugging these two expressions into the state-dependent PLDM force

$$\mathbf{F}_e = -\frac{1}{4}\sum_{\alpha\beta}\nabla V_{\alpha\beta}(\mathbf{R})[p_\alpha p_\beta + q_\alpha q_\beta + p'_\alpha p'_\beta + q'_\alpha q'_\beta]$$

we obtain the nuclear force in the QD representation as follows

$$\begin{aligned}\mathbf{F}_e &= -\frac{1}{4}\sum_{ij\alpha\beta} C_{i\alpha}\nabla V_{\alpha\beta}(\mathbf{R})C_{j\beta}[p_i p_j + q_i q_j + p'_i p'_j + q'_i q'_j] \\ &= -\frac{1}{4}\sum_{ij}\nabla V_{ij}(\mathbf{R})[p_i p_j + q_i q_j + p'_i p'_j + q'_i q'_j]\end{aligned} \tag{18}$$

The current equations of motion for QD-PLDM are closely related to those used in the adiabatic Forward−Backward (FB)-QCLE,[24] with the same nuclear force expression. In addition, the QD-PLDM force shares a similar feature with the force in the recently developed kinematically transformed KT-SQC,[22] where the second-derivative couplings explicitly vanish. However, both KT-SQC and adiabatic FB-QCLE do explicitly require computing nonadiabatic coupling elements $\langle\Phi_j(\mathbf{R}(t))|\frac{\partial}{\partial t}\Phi_i(\mathbf{R}(t))\rangle = \mathbf{d}_{ji}\dot{\mathbf{R}}$ in order to propagate the mapping equations. Thus, these two approaches might encounter numerical instability when these couplings are highly peaked.

Finally, we would like to emphasize that the accuracy of QD-PLDM will be limited by PLDM, i.e., the validity of partial linearization approximation. Rather, the QD propagation scheme provides a convenient framework that allows diabatic dynamics approaches to directly uses electronic energies and gradients in the adiabatic representation for quantum dynamics propagation.

Details of Model Calculations. *Model Systems.* For the model nonadiabatic systems investigated in this paper, the exact expression of the Hamiltonian $\hat{H} = \hat{T} + \sum_{\alpha\beta}V_{\alpha\beta}(\hat{\mathbf{R}})|\alpha\rangle\langle\beta|$ is available in the diabatic representation $\{|\alpha\rangle,|\beta\rangle\}$. These expressions, together with the model parameters are provided in the Supporting Information.

The matrix elements of the electronic Hamiltonian $V_{\alpha\beta}(\mathbf{R}(t))$ and the nuclear gradients in the diabatic representation $\nabla V_{\alpha\beta}(\mathbf{R}(t))$ are available and directly used in PLDM propagations. For QD-PLDM propagations, the adiabatic basis $\{|\Phi_i(\mathbf{r};\mathbf{R}(t))\rangle\}$ is obtained by diagonalizing the $V_{\alpha\beta}(\mathbf{R}(t))$ matrix, which is used as the QD basis. The matrix elements of the electronic Hamiltonian and nuclear gradients

DOI: 10.1021/acs.jctc.7b01178
J. Chem. Theory Comput. 2018, 14, 1828−1840

are evaluated using eqs 6−8 and eq 9, respectively. Alternatively, these elements can be easily computed by taking advantage of the available diabatic basis, for example, as $V_{ij}(\mathbf{R}(t)) = \sum_{\alpha\beta}\langle\Phi_i(\mathbf{r};\mathbf{R_0})|\alpha\rangle\ V_{\alpha\beta}(\mathbf{R}(t))\langle\beta|\Phi_j(\mathbf{r};\mathbf{R_0})\rangle$.

The initial conditions for all of the model systems are $\hat{\rho}(0) = |\nu\rangle\langle\nu|\otimes\hat{\rho}_{\mathbf{R}}$, where $|\nu\rangle$ indicates the initial electronic diabatic state and $\hat{\rho}_{\mathbf{R}}$ represents the initial nuclear density operator. For nonadiabatic scattering and photodissociation calculations presented in Figures 2−4, we use $\hat{\rho}_{\mathbf{R}} = |\chi\rangle\langle\chi|$, where $\langle\mathbf{R}|\chi\rangle = \left(\frac{2\Gamma}{\pi}\right)^{1/4} e^{-(\Gamma/2)(\mathbf{R}-\mathbf{R}_0)^2+i/\hbar\mathbf{P}_0(\mathbf{R}-\mathbf{R}_0)}$ represents a Gaussian wavepacket centered around $\mathbf{R_0}$ and $\mathbf{P_0}$ with a width Γ. For the condensed-phase model calculations presented in Figures 5 and 6, we assume that each nuclear DOF is represented by a harmonic mode that has a canonical thermal density $\rho_{\mathbf{R}} = \mathrm{Tr}_{\mathbf{R}}[\hat{\rho}_{\mathbf{R}}] = \mathrm{Tr}_{\mathbf{R}}[e^{-(\frac{\hat{\mathbf{P}}^2}{2m}+\frac{m}{2}\omega^2\hat{\mathbf{R}}^2)/k_BT}]$.

For PLDM and QD-PLDM calculations, the initial conditions for nuclear and mapping DOFs are generated from $[\hat{\rho}(0)^{\mathrm{W}}_{\gamma\mu}]$, and G_0 and G'_0, respectively. Here, the partial Wigner transformations $[\hat{\rho}(0)^{\mathrm{W}}_{\gamma\mu}] = (\rho_{\mathbf{R}})^{\mathrm{W}}\delta_{\gamma\nu}\delta_{\mu\nu}$ can be performed analytically with the $\hat{\rho}_{\mathbf{R}}$ provided above, yielding

$$(\rho_{\mathbf{R}})^{\mathrm{W}} = \frac{1}{\pi}e^{-(\Gamma/2)(\mathbf{R}-\mathbf{R}_0)^2-(\mathbf{P}-\mathbf{P}_0)^2/(\Gamma/2)}$$

for the Gaussian wavepacket and $(\rho_{\mathbf{R}})^{\mathrm{W}} = 2\tanh(\omega/2k_BT)\ e^{-\tanh(\omega/2k_BT)[m\omega(\mathbf{R}-\mathbf{R}_0)^2+(\mathbf{P}-\mathbf{P}_0)^2/m\omega]}$ for the harmonic bath at a finite temperature. The initial conditions of the forward and backward mapping DOFs are sampled from G_0, and G'_0, except for the results presented in Figures 3 and 4 where focused initial conditions,[65] $q_\mu = q'_\mu = \delta_{\mu\nu}$ and $p_\mu = -p'_\mu = \delta_{\mu\nu}$, are used to facilitate the convergence of the calculations. We used 10^5 trajectories for calculations with sampled initial conditions and 10^4 trajectories for calculations with the focused initial conditions.

Atomistic Systems. We perform on-the-fly calculations for the photoinduced charge separation dynamics with a model organic photovoltaic (OPV) system. We use density the functional tight-binding (DFTB) method with self-consistent charge corrections for electronic structure calculations. DFTB has proven to provide accurate electronic structures for model OPV systems[66,67] Here, we perform the on-the-fly calculations at the DFTB3 level of theory,[68] with the 3ob-3−1 Slater−Koster parameter set[69] as implemented in the DFTB+ package.[70] Dispersion interaction between atoms are incorporated by using Lennard-Jones potential with UFF parameters.[71]

In this paper, we adapt a widely used approximation for simulating the photoinduced charge transfer dynamics. We assume that the time-dependent wave function for transferring a single electron can be expressed as a linear combination of the ground state DFTB molecular orbitals (MOs) (see Appendix A for more information). This approximation has proven to provide an accurate description of the photoinduced charge transfer dynamics.[28,72−76] To further reduce the computational cost, we truncate the size of the MO basis to a smaller set which contains LUMO to LUMO+9 orbitals. These are low-lying orbitals that directly participate in the photoinduced charge transfer process. We have carefully checked the convergence of our truncation scheme compared to the propagation with the entire set of MOs with the results provided in the Supporting Information.

In the QD-PLDM scheme, the above approximation corresponds to using the ground state DFTB MOs as the QD basis to construct the classical mapping Hamiltonian in eq 14. The matrix elements of the electronic Hamiltonian are calculated from eqs 6−8. To evaluate $V_{ij}(\mathbf{R}(t_2))$ in eq 8, we need to compute the overlap between two bases $b_{ik} = \langle\ \Phi_i(\mathbf{r};\mathbf{R_0})|\Phi_k(\mathbf{r};\mathbf{R}(t_2))\rangle$. This can be easily computed in the atomic orbital (AO) basis, for example, $|\Phi_i(\mathbf{r};\mathbf{R_0})\rangle = \sum_\mu C_{\mu i}(\mathbf{R_0})|\varphi_\mu(\mathbf{r},\mathbf{R_0})\rangle$ with expansion coefficient $C_{\mu i}(\mathbf{R_0})$. Thus, the overlap between two adiabatic bases can be computed as

$$\langle\Phi_i(\mathbf{r};\mathbf{R_0})|\Phi_k(\mathbf{r};\mathbf{R}(t_2))\rangle = \sum_{\mu\nu} C_{\mu i}(\mathbf{R_0})C_{\nu k}(\mathbf{R}(t_2))S_{\mu\nu} \tag{19}$$

where $S_{\mu\nu} = \langle\varphi_\mu(\mathbf{r};\mathbf{R_0})|\varphi_\nu(\mathbf{r};\mathbf{R}(t_2))\rangle$ is the overlap between two AOs at two different time steps. These overlap integrals are evaluated with our in-house version of the DFTB+ code.

The initial electronic state is chosen to be one of the MOs of the entire system. To model the photoinduced charge transfer dynamics between donor and acceptor molecules, we choose the initial MO as $|\Phi_i(\mathbf{r};\mathbf{R})\rangle$, such that it maximizes the overlap $\langle\Phi^{\mathrm{D}}_{\mathrm{LUMO}}|\Phi_i(\mathbf{r};\mathbf{R})\rangle$. Here, $|\Phi^{\mathrm{D}}_{\mathrm{LUMO}}\rangle$ is the LUMO orbital of the donor moiety as obtained from the DFTB calculation of the isolated donor. This provides a reasonable single-electron picture of the localized photoexcitation of the system.[28,74] We use eq 19 to compute the overlap $\langle\Phi^{\mathrm{D}}_{\mathrm{LUMO}}|\Phi_i(\mathbf{r};\mathbf{R})\rangle$ and simply assume that $|\Phi^{\mathrm{D}}_{\mathrm{LUMO}}\rangle$ has zero expansion coefficients over the AOs on the acceptor moiety.

Between two consecutive short-time QD-PLDM propagations, we need to transform the mapping variables from the old QD basis $\{|\Phi_i(\mathbf{r};\mathbf{R}(t_1))\rangle\}$ to the new QD basis $\{|\Phi_k(\mathbf{r};\mathbf{R}(t_2))\rangle\}$. As discussed in the QD-PLDM theory section, this requires expressing QD state vectors $\{|\Phi_k(\mathbf{r};\mathbf{R}(t_2))\rangle\}$ in terms of the previous basis as

$$|\Phi_k(\mathbf{r};\mathbf{R}(t_2))\rangle = \sum_i \langle\Phi_i(\mathbf{r};\mathbf{R}(t_1))|\Phi_k(\mathbf{r};\mathbf{R}(t_2))\rangle|\Phi_i(\mathbf{r};\mathbf{R}(t_1))\rangle \tag{20}$$

However, the new QD vectors do not necessarily maintain their mutual orthogonality when they are expressed in terms of the previous QD basis. The reason is that $\{|\Phi_i(\mathbf{r};\mathbf{R}(t_1))\rangle\}$ is no longer a complete basis for representing $|\Phi_k(\mathbf{r};\mathbf{R}(t_2))\rangle$. Without a proper orthonormalization, the total population will gradually decay from unity. To alleviate this problem, we perform the Gram−Schmidt orthonormalization procedure among vectors $\langle\Phi(\mathbf{r};\mathbf{R}(t_1))|\Phi_k(\mathbf{r};\mathbf{R}(t_2))\rangle$ for all k. This is a valid procedure for single electron bases (MOs) used here. In future implementation, a similar procedure can be easily accomplished for many-electrons basis (for example, Slater determinants) by using the Löwdin orthogonalization method.[32,77,78]

With the time-dependent reduced density matrix $\rho_{ij}(t)$ obtained from QD-PLDM propagation, we characterize the photoinduced charge transfer dynamics by computing the time-dependent charge population on molecule N with the following expression[28,72]

$$P_N(t) = \mathrm{Re}\sum_{\mu\in N}^{\nu}\sum_{ij}\rho_{ij}(t)C_{\mu i}(\mathbf{R}(t))S_{\mu\nu}C_{\nu j}(\mathbf{R}(t)) \tag{21}$$

with the AO coefficients $C_{\mu i}(\mathbf{R}(t))$ and AO overlap matrix $S_{\mu\nu} = \langle\varphi_\mu(\mathbf{r},\mathbf{R}(t))|\varphi_\nu(\mathbf{r},\mathbf{R}(t))\rangle$. We emphasize that our focus in this paper is to examine the accuracy of the QD propagation scheme, rather than providing the physical dynamics of the

DOI: 10.1021/acs.jctc.7b01178
J. Chem. Theory Comput. 2018, 14, 1828−1840

photoinduced charge transfer process. Thus, we choose to adapt the classical path approximation (CPA)[28,53,72,76,79] that ignores the back reaction from electronic nonadiabatic transitions to the motion of the nuclei. Based on this approximation, we use the DFTB ground state force, $\mathbf{F}_0$, to propagate the motion of the nuclei. The mapping variables are propagated with the QD-PLDM equations of motion that parametrically depend upon the nuclear positions. In addition, we only present the quantum dynamics results with a *single* nuclear trajectory in order to conveniently demonstrate the accuracy of QD-PLDM. Further, we choose to use the classical Boltzmann distribution instead of the Wigner distribution (as required by PLDM) to simplify our calculations.

We generate the initial conditions with the following procedure. First, we equilibrate the system under the NVT ensemble with the Nosé−Hoover chain thermostat as implemented in the DFTB+ package for 30 ps with a 0.5 fs nuclear time step. The trajectory is further equilibrated with 5 ps-long NVE dynamics, which produces the initial condition for the single nuclear trajectory. For QD-PLDM quantum dynamics propagation, the nuclear time step is 0.1 fs, and the electronic time step for propagating the mapping equations is 10^{-3} fs. The initial conditions of the mapping variables are sampled from the Husimi distribution governed by $G_0(\mathbf{q}, \mathbf{p})$ and $G_0'(\mathbf{q}', \mathbf{p}')$, with 10^4 various configurations (mapping trajectories). The same numerical result is also obtained by using a single mapping trajectory with focused initial conditions.[65]

Under the above simplifications, QD-PLDM equations generate exactly the same results as obtained by numerically solving TDSE.[56,57] Thus, we directly compare the results obtained from QD-PLDM with the numerical solution of TDSE in the adiabatic representation to validate the accuracy of the QD propagation scheme.

RESULTS AND DISCUSSIONS

Figure 2 presents the results of Tully's three nonadiabatic scattering systems[5] with (a) single avoided crossing (Tully's model I), (b) dual avoided crossing (Tully's model II), and (c) extended coupling with reflection (Tully's model III). These results are obtained from diabatic PLDM propagation, QD-PLDM, and numerical exact split-operator Fourier transform method. Initial nuclear conditions are sampled from a Gaussian wavepacket, with Γ = 1 au, R_0 = −9.0 au, and P_0 = 30. a.u. Figure 2a−c provides both population ($\rho_{11}(t)$ in red and $\rho_{22}(t)$ in green), as well as electronic coherence (Re[$\rho_{12}(t)$] in magenta and Im[$\rho_{12}(t)$] in blue). QD-PLDM gives the same results as those obtained from PLDM, both of which are almost identical with the numerical exact results. Finally, Figure 2d presents the asymptotic diabatic population of Tully's model II as a function of the center momenta $P_0 = \hbar k$ for the initial nuclear wavepacket. Again, QD-PLDM provides the same

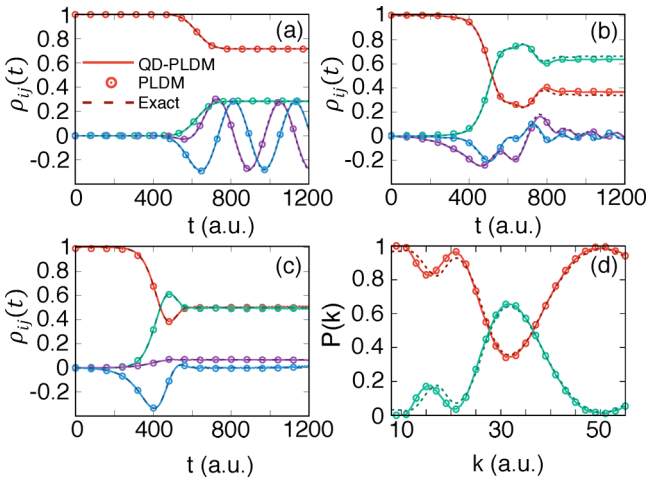

Figure 2. Diabatic state population of Tully's nonadiabatic scattering models with (a) model I, (b) model II, and (c) model III. Results are obtained from PLDM (open circles), QD-PLDM (solid), and numerical exact calculations (dash). (d) Asymptotic diabatic population of model II as a function of various center momenta $P_0 = \hbar k$ of the initial nuclear wavepacket.

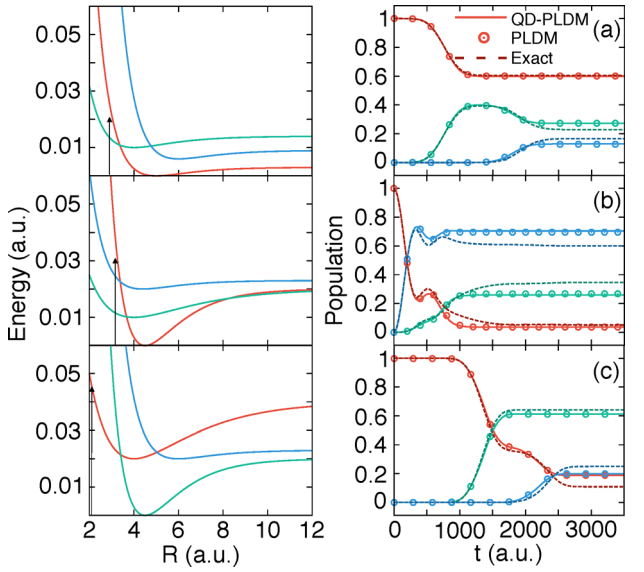

Figure 3. (Left) Diabatic potentials for photodissociation models with black arrows indicating the vertical Franck−Condon photoexcitations. (Right) The corresponding diabatic state populations, obtained from PLDM (open circles), QD-PLDM (solid lines), and numerical exact calculations (dashed lines).

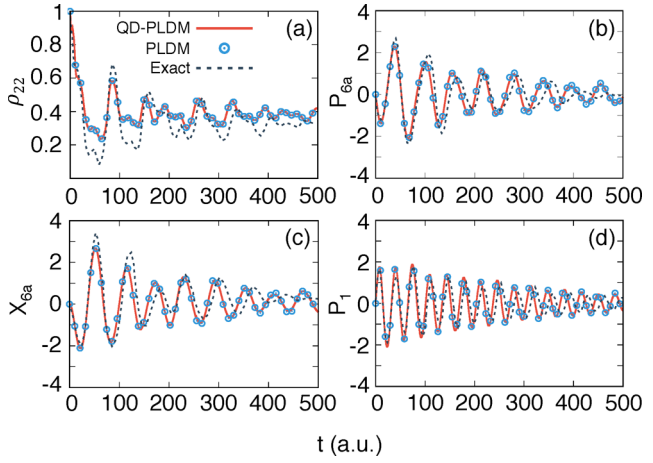

Figure 4. Quantum dynamics in a conical intersection model of pyrazine with (a) diabatic population of state $|2\rangle$, (b) average momentum of the 6*a* mode, (c) average momentum of the symmetric mode, and (d) average position of the 6a mode. Results are obtained from PLDM (open circles), QD-PLDM (solid lines), and numerical exact calculations (dashed lines).

DOI: 10.1021/acs.jctc.7b01178
J. Chem. Theory Comput. 2018, 14, 1828−1840

results as the diabatic PLDM, and both are close to the numerical exact ones.

Figure 3 presents the results of photodissociation dynamics of three coupled Morse potentials.[80,81] The left panels provide the diabatic potentials, with state $|1\rangle$ in red, $|2\rangle$ in green, and $|3\rangle$ in blue. The vertical arrows indicate the positions of photoexcitations that promote the ground state wavepacket up to the diabatic state $|1\rangle$. Figure 3a−c on the right-hand side presents the population dynamics obtained from PLDM, QD-PLDM, and numerical exact calculations, with the same color coding used in the potential curves on the left-hand side. In all three test cases, QD-PLDM yields the same results as PLDM, both of which are close to the numerical exact results.

Figure 4 presents the results for a two-state, three-mode conical intersection model.[82−84] Here, the three modes are indicated as $R_j \in \{R_1, R_{6a}, R_{10a}\}$, and the model Hamiltonian has the following form

$$\hat{H} = \sum_j \frac{1}{2}[P_j^2 + \omega_j^2 R_j^2] + \sum_\alpha \left[E_\alpha + \sum_j c_j^\alpha R_j\right]|\alpha\rangle\langle\alpha| + \lambda R_{10a}[|1\rangle\langle 2| + |2\rangle\langle 1|]$$

All of the parameters are provided in the Supporting Information. The nonadiabatic coupling element $\langle\Phi_1(\mathbf{R}(t))|\frac{\partial}{\partial t}|\Phi_2(\mathbf{R}(t))\rangle$ and derivative coupling vector diverge near the conical intersection, creating numerical challenges for directly solving TDSE (eq 24). The QD scheme avoids this challenge because it only requires $\langle\Phi_1(\mathbf{R}(t_1))|\Phi_2(\mathbf{R}(t_2))\rangle$ for the basis transformation during the dynamical propagation. Figure 4 demonstrates that QD-PLDM exactly reproduces the diabatic PLDM results, with (a) the diabatic population of state $|2\rangle$ and (b)−(d) expectation values of the nuclear positions and momenta. In addition, both PLDM and QD-PLDM provide reasonable accuracy compared to the numerical exact results.

To test the QD scheme for condensed-phase simulations, now we move to a spin-boson Hamiltonian expressed as $\hat{H} = \sum_j[\hat{P}_j^2/2 + \omega_j^2\hat{R}_j^2/2 + c_j\hat{R}_j\,\hat{\sigma}_z] + \epsilon\,\hat{\sigma}_z/2 + \Delta\hat{\sigma}_x$, with electronic bias ϵ, electronic coupling Δ, and the system-bath coupling c_j for a given spectral density $J(\omega) = \frac{\pi}{2}\sum_j \frac{c_j^2}{\omega_j}\delta(\omega - \omega_j)$. Here, we use 100 discretized harmonic modes to sample the spectral density $J(\omega) = \frac{\pi}{2}\xi\omega e^{-\omega/\omega_c}$, where ξ is the Kondo parameter and ω_c is the cutoff frequency (peak of the spectral density). For the model calculations in this paper, we use $\Delta = 1$ and $\omega_c = 2.5$ (Figure 5a−c) or $\omega_c = 1$ (Figure 5d). The Wigner distribution for the bath modes is centered around $\mathbf{R}_{0j} = -c_j/\omega_j^2$ and $\mathbf{P}_0 = 0$.

Figure 5 presents the results of spin-boson model with various electronic biases and temperatures. QD-PLDM provides identical results compared to PLDM in all cases, which are close to the exact results obtained from quasi-adiabatic propagator path integral (QUAPI) calculations.[85,86] The most significant deviation between QD-PLDM and exact result can be seen in panel (c), where linearization approximation becomes less accurate at low temperature. However, we can always systematically improve the accuracy of the results with an iterative propagation scheme,[14,23] which can be easily implemented in the QD representation.

Figure 6 presents the quantum dynamics results for an excitation energy transfer (EET) model system.[87] This Frenkel exciton model is expressed as $\hat{H} = \hat{H}_e + \hat{H}_{ep}$. The electronic part of the Hamiltonian is $\hat{H}_e = \sum_\alpha \epsilon_\alpha|\alpha\rangle\langle\alpha| + \sum_{\alpha\neq\gamma}\Delta_{\alpha\gamma}|\alpha\rangle\langle\gamma|$, with

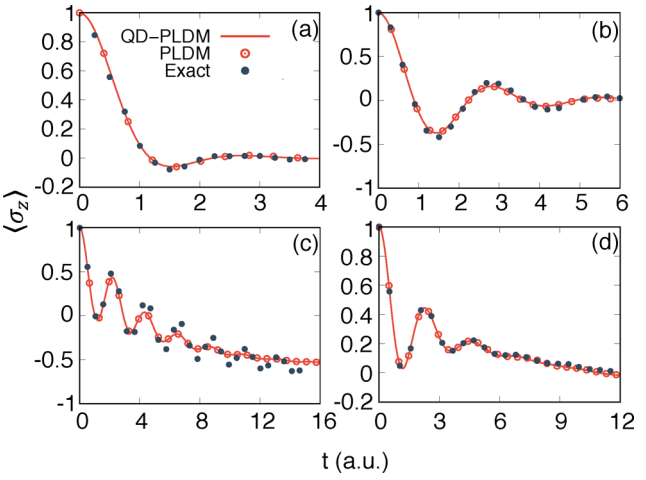

Figure 5. Quantum dynamics for spin-boson model with various bias ϵ and temperature with (a) $\epsilon = 0$, $(k_BT)^{-1} = 0.1$, $\xi = 0.09$, (b) $\epsilon = 0$, $(k_BT)^{-1} = 0.4$, $\xi = 0.13$, (c) $\epsilon = 1$, $(k_BT)^{-1} = 5.0$, $\xi = 0.1$, and (d) $\epsilon = 1$, $(k_BT)^{-1} = 0.25$, $\xi = 0.1$. Results are obtained from PLDM (open circles), QD-PLDM (solid lines), and numerical exact calculations (filled circles).

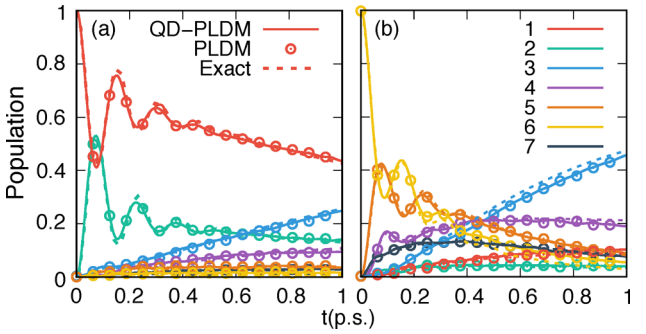

Figure 6. Population dynamics for excitation energy transfer (EET) process in a model Fenna−Matthews−Olson (FMO) complex. Diabatic state populations with an initial excitation on (a) state $|1\rangle$ or (b) state $|6\rangle$ are presented. Results are obtained from PLDM (open circles), QD-PLDM (solid lines), and numerical exact calculations (dashed lines).

singlet excitation energy ϵ_α on chromophore α and electronic coupling $\Delta_{\alpha\gamma}$ between two single excitations $|\alpha\rangle$ and $|\gamma\rangle$. The electron−phonon interaction Hamiltonian is

$$\hat{H}_{ep} = \sum_\alpha \sum_{j_\alpha}\left[\frac{1}{2}(\hat{P}_{j_\alpha}^2 + \omega_{j_\alpha}^2\hat{R}_{j_\alpha}^2) + c_{j_\alpha}\hat{R}_{j_\alpha}|\alpha\rangle\langle\alpha|\right]$$

where each state $|\alpha\rangle$ is coupled to a set of independent harmonic bath modes $\{R_{j_\alpha}\}$. Here, we use the model parameters of the Fenna−Matthews−Olson (FMO) complex that contains seven chromophores.[87] In addition, we use 60 modes to sample the spectral density $J(\omega) = 2\lambda\omega\tau/(1 + (\omega\tau)^2)$ for each bath, where the reorganization energy is $\lambda = 35\ \text{cm}^{-1}$, and the solvent response time is $\tau = 50$ fs. The parameters for $\hat{H}_e$ as well as the sampling procedure for the spectral density are provided in the Supporting Information. The Wigner distribution for each bath mode is centered around $\mathbf{R}_0 = 0$ and $\mathbf{P}_0 = 0$. In Figure 6, the diabatic state population obtained from PLDM and QD-PLDM are compared to the exact results obtained from hierarchy equations of motion (HEOM) approach,[87,88] with initial excitation from (a) state $|1\rangle$ and (b) state $|6\rangle$. As can be

DOI: 10.1021/acs.jctc.7b01178
J. Chem. Theory Comput. 2018, 14, 1828−1840

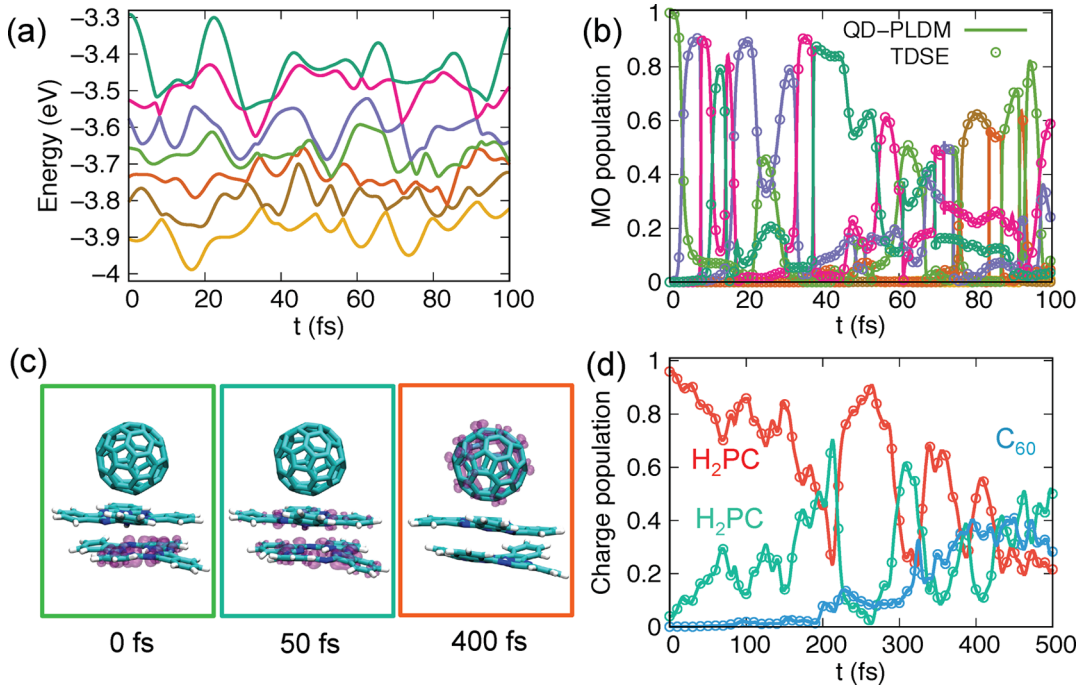

Figure 7. (a) Time-dependent MO energies (LUMO to LUMO+6) in a $2H_2$ Pc/C_{60} model system. (b) MO populations of the corresponding orbitals with the same color coding as in panel (a), obtained from QD-PLDM (solid lines) and the numerical integration of TDSE (open circles). (c) The electron density of the most populated MO at a given time, with boxes that have the same color coding as in panel (a) to indicate the corresponding MOs. (d) Time-dependent charge populations (eq 21) on each H_2PC molecule (red and green) and C_{60} moiety (blue) computed with QD-PLDM (solid lines) and the numerical integration of TDSE (open circles).

clearly seen, QD-PLDM exactly reproduces PLDM results, which are almost identical to the numerical exact results.

Finally, Figure 7 presents the results of the on-the-fly quantum dynamics in a model phthalocyanine dimer/fullerene ($2H_2$Pc/C_{60}) system. This system was recently explored as a model to understand photoinduced charge transfer dynamics in organic photovoltaics.[89,90] Figure 7a presents the time-dependent MO energies of LUMO to LUMO+6, computed from a single nuclear trajectory. Figure 7b presents the MO populations (adiabatic populations) obtained from QD-PLDM (solid lines) and numerical solution of TDSE (open circles), with details presented in Appendix A. The QD-PLDM scheme provides identical results compared to TDSE, as expected under this single trajectory, classical path limit. Figure 7c presents the electron density of the most populated MO at a given time, with boxes that have the same color coding in panel (a) to indicate the corresponding MOs. Figure 7d presents the time-dependent charge population (eq 21) on each H_2Pc molecule as well as on C_{60} moiety computed from the QD-PLDM scheme (solid lines), which is same as obtained from the numerical solution of TDSE (open circles). Note that the single nuclear trajectory result presented here is not physically meaningful; the purpose of this calculation is to validate the accuracy of QD propagation scheme.

CONCLUSIONS

We have developed a quasi-diabatic (QD) scheme that allows interfacing diabatic quantum dynamics approaches with commonly used adiabatic electronic structure calculations. This scheme uses crude adiabatic states as the quasi-diabatic basis during a short-time quantum propagation, thus taking advantage of both the compactness of QD basis obtained from adiabatic electronic structure calculations as well as the diabatic nature of the QD basis for quantum dynamics propagation. Between two consecutive short-time propagations, the electronic state basis is transformed from the old to the new QD representation. Using a partial linearized path integral approach as one particular example, we have demonstrated the accuracy of the QD scheme with a wide range of model nonadiabatic problems as well as the on-the-fly model calculations. This study opens the possibility to combine accurate diabatic quantum dynamics methods with adiabatic electronic structure calculations for on-the-fly quantum dynamics propagation.

APPENDIX A: NUMERICAL METHODS FOR SOLVING TIME-DEPENDENT SCHRÖDINGER EQUATION

Here, we provide the numerical method for solving the time-dependent Schrödinger equation (TDSE) in the adiabatic representation. For atomistic calculations in this paper, TDSE is governed by a predetermined nuclear trajectory $\mathbf{R}(t)$, with

$$i\hbar\frac{\partial}{\partial t}|\Psi(\mathbf{r};\,\mathbf{R}(t),\,t)\rangle = \hat{V}(\hat{\mathbf{r}};\,\mathbf{R}(t))|\Psi(\mathbf{r};\,\mathbf{R}(t),\,t)\rangle \tag{22}$$

To obtain the numerical solution of the above equation, we assume that this time-dependent wave function can be expanded as a linear combination of the instantaneous molecular orbitals (adiabatic state, single particle basis)

$$|\Psi(\mathbf{r};\,\mathbf{R}(t),\,t)\rangle = \sum_i c_i(t)|\Phi_i(\mathbf{r};\,\mathbf{R}(t))\rangle \tag{23}$$

where $c_i(t)$ is the time-dependent expansion coefficient. Plugging the above ansatz into TDSE (eq 22), we have the following differential equation for the time-dependent expansion coefficients

DOI: 10.1021/acs.jctc.7b01178
J. Chem. Theory Comput. 2018, 14, 1828−1840

$$\dot{c}_j(t) = -\frac{i}{\hbar}c_j(t)E_j(\mathbf{R}(t)) - \sum_i c_i(t)\langle\Phi_j(\mathbf{r};\mathbf{R}(t))|\frac{\partial}{\partial t}\Phi_i(\mathbf{r};\mathbf{R}(t))\rangle \quad (24)$$

Note that the nonadiabatic coupling elements

$$\langle\Phi_j(\mathbf{r};\mathbf{R}(t))|\frac{\partial}{\partial t}\Phi_i(\mathbf{r};\mathbf{R}(t))\rangle$$

are related to the derivative coupling vectors through following relation

$$\langle\Phi_j(\mathbf{R}(t))|\frac{\partial}{\partial t}\Phi_i(\mathbf{r};\mathbf{R}(t))\rangle = \langle\Phi_j(\mathbf{r};\mathbf{R}(t))|\nabla|\Phi_i(\mathbf{r};\mathbf{R}(t))\rangle\dot{\mathbf{R}} \quad (25)$$

Here, we directly solve eq 24 with the fourth-order Runge−Kutta numerical integration method.

To compute the nonadiabatic couplings (eq 25), we adapt a well-established approximation[40]

$$\langle\Phi_j|\frac{\partial}{\partial t}\Phi_i\rangle = \frac{1}{2\tau}\left[\langle\Phi_j(t)|\Phi_i(t+\tau)\rangle - \langle\Phi_j(t+\tau)|\Phi_i(t)\rangle\right] \quad (26)$$

where we use the shorthand notation $|\Phi_j(t)\rangle \equiv |\Phi_j(\mathbf{r};\mathbf{R}(t))\rangle$. This quantity needs to be carefully calculated by following the random phases generated from electronic structure calculations for the MOs.[26,27,91] We should note that there is a recently developed norm-preserving interpolation scheme[37,38] which outperforms the linear interpolation scheme presented above and provides a more stable integration of TDSE.

We perform DFTB calculations to obtain the time-dependent MOs. These MOs are expressed as linear combinations of the atomic orbitals (AOs) as $|\Phi_i(\mathbf{r};\mathbf{R}(t))\rangle = \sum_\mu C_{\mu i}(\mathbf{R}(t))|\varphi_\mu(\mathbf{r},\mathbf{R})\rangle$, with $C_{\mu i}(\mathbf{R}(t))$ obtained from solving DFTB eigenequations. Thus, the overlap between two adiabatic basis in eq 26 can be computed as

$$\langle\Phi_j(\mathbf{r};\mathbf{R}(t+\tau))|\Phi_i(\mathbf{r};\mathbf{R}(t))\rangle = \sum_{\mu\nu} C_{\mu j}(\mathbf{R}(t+\tau))C_{\nu i}(\mathbf{R}(t))S_{\mu\nu}(t+\tau,t) \quad (27)$$

Here, $S_{\mu\nu}(t+\tau,t)$ is the overlap between two atomic orbitals (AOs) at two different time steps

$$S_{\mu\nu}(t+\tau,t) = \langle\varphi_\mu(\mathbf{r},\mathbf{R}(t+\tau))|\varphi_\nu(\mathbf{r},\mathbf{R}(t))\rangle \quad (28)$$

These AO overlap integrals are explicitly evaluated with our in-house version of DFTB+ code.

In addition, we provide an alternative numerical procedure that explicitly avoids computing nonadiabatic couplings in eq 26. Starting with an ansatz that propagates the wave function from t_1 to t_2 with a duration $\tau = t_2 - t_1$

$$|\Psi(\mathbf{r};\mathbf{R}(t_2),t_2)\rangle = e^{-i\tau/\hbar\hat{V}(\hat{\mathbf{r}};\mathbf{R}(t_1))}|\Psi(\mathbf{r};\mathbf{R}(t_1),t_1)\rangle \quad (29)$$

and plugging the time-dependent wave function (eq 23) into the above equation, we have

$$|\Psi(\mathbf{r};\mathbf{R}(t_2),t_2)\rangle = e^{-i\tau/\hbar\hat{V}(\hat{\mathbf{r}};\mathbf{R}(t_1))}\sum_i c_i(t_1)|\Phi_i(\mathbf{r};\mathbf{R}(t_1))\rangle \quad (30)$$

Operating $\hat{V}(\hat{\mathbf{r}};\mathbf{R}(t_1))$ on $|\Phi_i(\mathbf{r};\mathbf{R}(t_1))\rangle$ and projecting $\langle\Phi_j(\mathbf{r};\mathbf{R}(t_2))|$ on both sides of the equation, we obtain the time-dependent expansion coefficients as follows

$$c_j(t_2) = \sum_i c_i(t_1)e^{-i\tau/\hbar E_i(\mathbf{R}(t_1))}\langle\Phi_j(\mathbf{r};\mathbf{R}(t_2))|\Phi_i(\mathbf{r};\mathbf{R}(t_1))\rangle \quad (31)$$

A symmetric version of this scheme has been previously developed to solve TDSE,[25−28] which is closely related to the Magnus expansion[25,41] and the QD scheme[30] for integrating TDSE. This scheme removes all possible singularities associated with the nonadiabatic couplings by using $\langle\Phi_j(\mathbf{r};\mathbf{R}(t_2))|\Phi_i(\mathbf{r};\mathbf{R}(t_1))\rangle$, instead of explicitly evaluating $\langle\Phi_j(\mathbf{R}(t))|\frac{\partial}{\partial t}\Phi_i(\mathbf{r};\mathbf{R}(t))\rangle$. Thus, it provides a more stable integration of TDSE when nonadiabatic couplings are highly peaked. Both schemes provide the same numerical results for the model presented in this paper, with a 0.1 fs time step.

We briefly comment on two crucial aspects of the propagation scheme outlined in eqs 30 and 31. First, it is easy to show that this short-time propagation scheme is equivalent to the direct numerical solution of the TDSE. Let $t_1 = t$, $t_2 = t + \tau$ and expand the terms $e^{-i\tau/\hbar E_i(\mathbf{R}(t))}$ and $\langle\Phi_j(\mathbf{r};\mathbf{R}(t+\tau))|$ of eq 31 up to the linear order with respect to τ as follows

$$c_j(t+\tau) = \sum_i c_i(t)\left(1 - \frac{i\tau}{\hbar}E_i(\mathbf{R}(t))\right) \times \left(\langle\Phi_j(\mathbf{r};\mathbf{R}(t))| + \tau\left\langle\frac{\partial}{\partial t}\Phi_j(\mathbf{r};\mathbf{R}(t))\right|\right)|\Phi_i(\mathbf{r};\mathbf{R}(t))\rangle \quad (32)$$

Also notice the fact that

$$\frac{\partial}{\partial t}\langle\Phi_j(\mathbf{r};\mathbf{R}(t))|\Phi_i(\mathbf{r};\mathbf{R}(t))\rangle = \frac{\partial}{\partial t}\delta_{ij} = 0 \quad (33)$$

which leads to

$$\langle\frac{\partial}{\partial t}\Phi_j(\mathbf{r};\mathbf{R}(t))|\Phi_i(\mathbf{r};\mathbf{R}(t))\rangle = -\langle\Phi_j(\mathbf{r};\mathbf{R}(t))|\frac{\partial}{\partial t}\Phi_i(\mathbf{r};\mathbf{R}(t))\rangle$$

In addition, using the relations $\dot{c}_j(t) = [c_j(t+\tau) - c_j(t)]/\tau$ and $\langle\Phi_j(\mathbf{r};\mathbf{R}(t))|\Phi_i(\mathbf{r};\mathbf{R}(t))\rangle = \delta_{ij}$, eq 32 can be rewritten (up to linear order of τ) as eq 24.

Second, this propagation scheme is closely related to the mapping variables propagation in the QD-PLDM scheme that we have introduced in the main text. Based on the MMST mapping relation, we have $c_j = \left(q_j + ip_j\right)/\sqrt{2}$. Plugging this expression into eq 31, we have the following equations for mapping variables

$$q_j(t_2) = \sum_i \langle\Phi_j(\mathbf{r};\mathbf{R}(t_2))|\Phi_i(\mathbf{r};\mathbf{R}(t_1))\rangle \times [q_i(t_1)\cos(E_i(\mathbf{R}(t_1))\tau) + p_i(t_1)\sin(E_i(\mathbf{R}(t_1))\tau)]$$

$$p_j(t_2) = -\sum_i \langle\Phi_j(\mathbf{r};\mathbf{R}(t_2))|\Phi_i(\mathbf{r};\mathbf{R}(t_1))\rangle \times [q_i(t_1)\sin(E_i(\mathbf{R}(t_1))\tau) - p_i(t_1)\cos(E_i(\mathbf{R}(t_1))\tau)] \quad (34)$$

Under the limit $\tau \to 0$, $V_{ij}(\mathbf{R}) \to 0$, the classical mapping Hamiltonian used in QD-PLDM becomes

$$h_m(\mathbf{R},\mathbf{p},\mathbf{q}) = \frac{1}{2}\sum_i E_i(\mathbf{R})(p_i^2 + q_i^2)$$

DOI: 10.1021/acs.jctc.7b01178
J. Chem. Theory Comput. 2018, 14, 1828−1840

The mapping variables will evolve as free harmonic oscillators (due to the zero electronic coupling elements) with the corresponding time-dependent evolution appearing in the square brackets of eq 34. The rest of the expressions correspond to the basis transform performed in step 7 of the QD-PLDM scheme in the main text.

APPENDIX B: MMST HAMILTONIAN IN ADIABATIC REPRESENTATION

Here, we briefly outline the adiabatic MMST Hamiltonian. Applying mapping representation for the adiabatic states $|\Psi_i(\mathbf{R})\rangle\langle\Psi_j(\mathbf{R})| \rightarrow \hat{a}_i^\dagger \hat{a}_j$, the "vibronic Hamiltonian" operator in eq 3 can be written as[23] $\hat{H} = \frac{\hat{\mathbf{P}}^2}{2M} + \hat{h}_m$, where

$$\hat{h}_m = \frac{1}{2}\sum_{ij}\left[E_i(\mathbf{R})\delta_{ij} - \frac{D_{ij}(\mathbf{R})}{2M}\right](\hat{q}_i\hat{q}_j + \hat{p}_i\hat{p}_j - \delta_{ij}) + \frac{1}{2}\sum_{ij}\frac{\hat{\mathbf{P}}}{M}\mathbf{d}_{ij}(\mathbf{R})(\hat{q}_i\hat{p}_j - \hat{p}_i\hat{q}_j) \tag{35}$$

Note that the vibronic Hamiltonian in eq 3 can also be written as[22]

$$\hat{H} = \sum_i E_i(\mathbf{R})|\Phi_i(\mathbf{r};\mathbf{R})\rangle\langle\Phi_i(\mathbf{r};\mathbf{R})| + \sum_{ij}\frac{1}{2M}(\hat{\mathbf{P}}\delta_{ij} - i\hbar\mathbf{d}_{ij}(\mathbf{R}))^2|\Phi_i(\mathbf{r};\mathbf{R})\rangle\langle\Phi_j(\mathbf{r};\mathbf{R})| \tag{36}$$

where the second-derivative coupling does not explicitly appear but will indeed arise[22] through the noncommutivity between $\hat{\mathbf{P}}$ and $\mathbf{d}_{ij}(\mathbf{R})$. Directly applying mapping representation for the adiabatic states of the above vibronic Hamiltonian in eq 36 leads to the standard adiabatic MMST Hamiltonian[8,22] as follows

$$\hat{H}_m = \frac{1}{2M}\left(\mathbf{P} + \sum_{ij}\hat{q}_i\hat{p}_j\mathbf{d}_{ij}(\mathbf{R})\right)^2 + \frac{1}{2}\sum_i E_i(\mathbf{R})(\hat{q}_i^2 + \hat{p}_i^2 - 1) \tag{37}$$

Approximate quantum dynamics approaches developed in the adiabatic mapping Hamiltonian will contain $\mathbf{d}_{ij}(\mathbf{R})$ and $D_{ij}(\mathbf{R})$ terms. For example, after evaluating the path-integral expression of the quantum propagator with the Hamiltonian in eq 35 or eq 37 and performing the linearization approximation, the forces that act on the nuclear DOF will contain ∇h_m or ∇H_m, which requires the evaluation of the $\mathbf{d}_{ij}(\mathbf{R})$ and $D_{ij}(\mathbf{R})$, or the gradients of them.

Thus, the MMST theory in the adiabatic representation significantly increases the complexity for quantum dynamics propagations. Recent theoretical developments have shown encouraging progress to remove these terms in the nuclear force expression through kinematic momentum transformation[22] or quantum-classical Liouville formalism.[24] In the QD propagation scheme, these derivative couplings vanish due to the diabatic nature of quasi-diabatic states, providing a convenient framework for quantum dynamics propagation.

ASSOCIATED CONTENT

Supporting Information

The Supporting Information is available free of charge on the ACS Publications website at DOI: 10.1021/acs.jctc.7b01178.

Model Hamiltonians and corresponding parameters used in the Results section; protocols of bath discretization for spin-boson model and FMO model; and additional results for validating MO truncation scheme used in atomistic system. (PDF)

AUTHOR INFORMATION

Corresponding Author

*E-mail: pengfei.huo@rochester.edu.

ORCID

Pengfei Huo: 0000-0002-8639-9299

Author Contributions

‡A.M. and S.S.Y. contributed equally to this work.

Notes

The authors declare no competing financial interest.

ACKNOWLEDGMENTS

This work was supported by the University of Rochester startup funds. Computing resources were provided by the Center for Integrated Research Computing (CIRC) at the University of Rochester. The authors thank Dr. Farnaz Shakib for helpful comments and a thorough reading of this manuscript and J. Sebastian Sandoval for preparing the model potential in the adiabatic representation.

REFERENCES

(1) Tully, J. C. Perspective: Nonadiabatic dynamics theory. *J. Chem. Phys.* **2012**, *137*, 22A301.

(2) Barbatti, M. Nonadiabatic Dynamics with Trajectory Surface Hopping Method. *Wiley Int. Rev. Comp. Mol. Sci.* **2011**, *1*, 620−633.

(3) Wang, L.; Akimov, A.; Prezhdo, O. V. Recent Progress in Surface Hopping: 2011−2015. *J. Phys. Chem. Lett.* **2016**, *7*, 2100−2112.

(4) Subotnik, J. E.; Jain, A.; Landry, B.; Petit, A.; Ouyang, W.; Bellonzi, N. Understanding the Surface Hopping View of Electronic Transitions and Decoherence. *Annu. Rev. Phys. Chem.* **2016**, *67*, 387−417.

(5) Tully, J. C. Molecular dynamics with Electronic Transitions. *J. Chem. Phys.* **1990**, *93*, 1061−1071.

(6) Parandekar, P. V.; Tully, J. C. Detailed balance in Ehrenfest mixed quantum-classical dynamics. *J. Chem. Theory Comput.* **2006**, *2*, 229−235.

(7) Schmidt, J. R.; Parandekar, P. V.; Tully, J. C. Mixed Quantum-Classical Euilibrium: Surface Hopping. *J. Chem. Phys.* **2008**, *129*, 044104.

(8) Ananth, N.; Venkataraman, C.; Miller, W. H. Semiclassical Description of Electronically Nonadiabatic Dynamics via the Initial Value Representation. *J. Chem. Phys.* **2007**, *127*, 084114.

(9) Miller, W. H.; Cotton, S. J. Classical Molecular Dynamics Simulation of Electronically Non-Adiabatic Processes. *Faraday Discuss.* **2016**, *195*, 9−30.

(10) Huo, P.; Coker, D. F. Communication: Partial Linearized Density Matrix Dynamics for Dissipative, Non-Adiabatic Quantum Evolution. *J. Chem. Phys.* **2011**, *135*, 201101.

(11) Menzeleev, A. R.; Bell, F.; Miller, T. F., III Kinetically Constrained Ring-Polymer Molecular Dynamics for Non-Adiabatic Chemical Reactions. *J. Chem. Phys.* **2014**, *140*, 064103.

(12) Ananth, N. Mapping variable ring polymer molecular dynamics: A path-integral based method for nonadiabatic processes. *J. Chem. Phys.* **2013**, *139*, 124102.

(13) Miller, W. H.; Cotton, S. J. Communication: Note on Detailed Balance in Symmetrical Quasi-Classical Models for Electronically Non-Adiabatic Dynamics. *J. Chem. Phys.* **2015**, *142*, 131103.

(14) Hsieh, C.-Y.; Kapral, R. Analysis of the forward-backward trajectory solution for the mixed quantum-classical Liouville equation. *J. Chem. Phys.* **2013**, *138*, 134110.

(15) Richardson, J. O.; Thoss, M. Communication: Nonadiabatic ring-polymer molecular dynamics. *J. Chem. Phys.* **2013**, *139*, 031102.
(16) Kelly, A.; Brackbill, N.; Markland, T. E. Accurate Nonadiabatic quantum dynamics on the cheap: Making the most of mean field theory with master equations. *J. Chem. Phys.* **2015**, *142*, 094110.
(17) van Voorhis, T.; Kowalczyk, T.; Kaduk, B.; Wang, L.-P.; Cheng, C.-L.; Wu, Q. The Diabatic Picture of Electron Transfer, Reaction Barriers, and Molecular Dynamics. *Annu. Rev. Phys. Chem.* **2010**, *61*, 149−170.
(18) Subotnik, J. E.; Alguire, E. C.; Ou, Q.; Landry, B. R.; Fatehi, S. The Requisite Electronic Structure Theory to Describe Photoexcited Nonadiabatic Dynamics: Nonadiabatic Derivative Couplings and Diabatic Electronic Couplings. *Acc. Chem. Res.* **2015**, *48*, 1340−1350.
(19) Kubas, A.; Hoffmann, F.; Heck, A.; Oberhofer, H.; Elstner, M.; Blumberger, J. Electronic Couplings for Molecular Charge Transfer: Benchmarking CDFT, FODFT, and FODFTB Against High-Level Ab Initio Calculations. *J. Chem. Phys.* **2014**, *140*, 104105.
(20) Zeng, X.; Hu, X.; Yang, W. Fragment-Based Quantum Mechanical/Molecular Mechanical Simulations of Thermodynamic and Kinetic Process of the Ru2-Ru3 Self-Exchange Electron Transfer. *J. Chem. Theory Comput.* **2012**, *8*, 4960−4967.
(21) Sirjoosingh, A.; Hammes-Schiffer, S. Diabatization Schemes for Generating Charge-Localized Electron-Proton Vibronic States in Proton-Coupled Electron Transfer Systems. *J. Chem. Theory Comput.* **2011**, *7*, 2831−2841.
(22) Cotton, S. J.; Liang, R.; Miller, W. H. On the Adiabatic Representation of Meyer-Miller Electronic-Nuclear Dynamics. *J. Chem. Phys.* **2017**, *147*, 064112.
(23) Huo, P.; Coker, D. F. Consistent Schemes for Non-Adiabatic Dynamics Derived from Partial Linearized Density Matrix Propagation. *J. Chem. Phys.* **2012**, *137*, 22A535.
(24) Hsieh, C.-Y.; Schofield, J.; Kapral, R. Forward-backward solution of the quantum-classical Liouville equation in the adiabatic mapping basis. *Mol. Phys.* **2013**, *111*, 3546−3554.
(25) Webster, F.; Rossky, P. J.; Friesner, R. A. Nonadiabatic Processes in Condensed Matter: Semi-Classical Theory and Implementation. *Comput. Phys. Commun.* **1991**, *63*, 494−522.
(26) Space, B.; Coker, D. Nonadiabatic Dynamics of Excited Excess Electrons in Simple Fluids. *J. Chem. Phys.* **1991**, *94*, 1976−1984.
(27) Yu, N.; Margulis, C.; Coker, D. Influence of Solvation Environment on Excited State Avoided Crossings and Photodissociation Dynamics. *J. Phys. Chem. B* **2001**, *105*, 6728−6737.
(28) Rego, L. G.; Batista, V. S. Quantum Dynamics Simulations of Interfacial Electron Transfer in Sensitized TiO2 Semiconductors. *J. Am. Chem. Soc.* **2003**, *125*, 7989−7997.
(29) Torres, A.; Oliboni, R. S.; Rego, L. G. Vibronic and Coherent Effects on Interfacial Electron Transfer Dynamics. *J. Phys. Chem. Lett.* **2015**, *6*, 4927−4935.
(30) Granucci, G.; Persico, M.; Toniolo, A. Direct semiclassical simulation of photochemical processes with semiempirical wave functions. *J. Chem. Phys.* **2001**, *114*, 10608−10615.
(31) Gao, X.; Geng, H.; Peng, Q.; Ren, J.; Yi, Y.; Wang, D.; Shuai, Z. Nonadiabatic Molecular Dynamics Modeling of the Intrachain Charge Transport in Conjugated Diketopyrrolo-Pyrrole Polymers. *J. Phys. Chem. C* **2014**, *118*, 6631−6640.
(32) Plasser, F.; Granucci, G.; Pittner, J.; Barbatti, M.; Persico, M.; Lischka, H. Surface Hopping Dynamics using a Locally Diabatic Formalism: Charge Transfer in the Ethylene Dimer Cation and Excited State Dynamics in the 2-Pyridone Dimer. *J. Chem. Phys.* **2012**, *137*, 22A514.
(33) Lee, M. K.; Huo, P.; Coker, D. F. Semiclassical Path Integral Dynamics: Photosynthetic Energy Transfer with Realistic Environment Interactions. *Annu. Rev. Phys. Chem.* **2016**, *67*, 639−668.
(34) Azumi, T.; Matsuzaki, K. What does the term "Vibronic Coupling" mean? *Photochem. Photobiol.* **1977**, *25*, 315−326.
(35) Ballhausen, C.; Hansen, A. Electronic Spectra. *Annu. Rev. Phys. Chem.* **1972**, *23*, 15−38.
(36) Longuet-Higgins, H. Some Recent Developments in the Theory of Molecular Energy Levels. In *Advances in Spectroscopy*, Volume II; Thompson, H. W., Ed.; Interscience Publishers, Ltd.: New York, 1961; p 429.
(37) Meek, G. A.; Levine, B. G. Evaluation of the Time-Derivative Coupling for Accurate Electronic State Transition Probabilities from Numerical Simulations. *J. Phys. Chem. Lett.* **2014**, *5*, 2351−2356.
(38) Jain, A.; Alguire, E.; Subotnik, J. E. An Efficient, Augmented Surface Hopping Algorithm That Includes Decoherence for Use in Large-Scale Simulations. *J. Chem. Theory Comput.* **2016**, *12*, 5256−5268.
(39) Meek, G. A.; Levine, B. G. The best of both Reps-Diabatized Gaussians on adiabatic surfaces. *J. Chem. Phys.* **2016**, *145*, 184103.
(40) Hammes-Schiffer, S.; Tully, J. C. Proton Transfer in Solution: Molecular Dynamics with Quantum Transitions. *J. Chem. Phys.* **1994**, *101*, 4657−4667.
(41) Pechukas, P.; Light, J. C. On the Exponential Form of Time-Displacement Operators in Quantum Mechanics. *J. Chem. Phys.* **1966**, *44*, 3897−3912.
(42) da Silva Oliboni, R.; Bortolini, G.; Torres, A.; Rego, L. G. C. A Nonadiabatic Excited State Molecular Mechanics/Extended Hückel Ehrenfest Method. *J. Phys. Chem. C* **2016**, *120*, 27688−27698.
(43) Cotton, S. J.; Miller, W. H. Symmetrical Windowing for Quantum States in Quasi-Classical Trajectory Simulations: Application to electronically non-adiabatic processes. *J. Chem. Phys.* **2013**, *139*, 234112.
(44) Miller, W. H.; Cotton, S. J. Communication: Wigner Functions in Action-Angle Variables, Bohr-Sommerfeld Quantization, the Heisenberg Correspondence Principle, and a Symmetrical Quasi-Classical Approach to the Full Electronic Density Matrix. *J. Chem. Phys.* **2016**, *145*, 081102.
(45) Cotton, S. J.; Miller, W. H. A New Symmetrical Quasi-Classical Model for Electronically Non-Adiabatic Processes: Application to the Case of Weak Non-Adiabatic Coupling. *J. Chem. Phys.* **2016**, *145*, 144108.
(46) Miller, W. H.; Cotton, S. J. The Symmetrical Quasi-Classical Model for Electronically Non-Adiabatic Processes Applied to Energy Transfer Dynamics in Site-Exciton Models of Light-Harvesting Complexes. *J. Chem. Theory Comput.* **2016**, *12*, 983−991.
(47) Hsieh, C.-Y.; Kapral, R. Nonadiabatic dynamics in open quantum-classical systems: Forward-backward trajectory solution. *J. Chem. Phys.* **2012**, *137*, 22A507.
(48) Kim, H.; Nassimi, A.; Kapral, R. Quantum-Classical Liouville Dynamics in the Mapping Basis. *J. Chem. Phys.* **2008**, *129*, 084102.
(49) Nassimi, A.; Bonella, S.; Kapral, R. Analysis of the quantum-classical Liouville equation in the mapping basis. *J. Chem. Phys.* **2010**, *133*, 134115.
(50) Kelly, A.; van Zon, R.; Schofield, J.; Kapral, R. Mapping Quantum-Classical Liouville Equation: Projectors and Trajectories. *J. Chem. Phys.* **2012**, *136*, 084101.
(51) Lambert, R.; Makri, N. Quantum-Classical Path Integral. I. Classical Memory and Weak Quantum Nonlocality. *J. Chem. Phys.* **2012**, *137*, 22A552.
(52) Lambert, R.; Makri, N. Quantum-classical path integral. II. Numerical Methodology. *J. Chem. Phys.* **2012**, *137*, 22A553.
(53) Makri, N. Quantum-Classical Path Integral: A Rigorous Approach to Condensed Phase Dynamics. *Int. J. Quantum Chem.* **2015**, *115*, 1209−1214.
(54) Walters, P. L.; Makri, N. Quantum-classical path integral simulation of ferrocene-ferrocenium charge transfer in liquid hexane. *J. Phys. Chem. Lett.* **2015**, *6*, 4959−4965.
(55) Meyer, H.; Miller, W. H. A Classical Analog for Electronic Degrees of Freedom in Nonadiabatic Collision Processes. *J. Chem. Phys.* **1979**, *70*, 3214−3223.
(56) Stock, G.; Thoss, M. Semiclassical Description of Nonadiabatic Quantum Dynamics. *Phys. Rev. Lett.* **1997**, *78*, 578−581.
(57) Thoss, M.; Stock, G. Mapping Approach to the Semiclassical Description of Nonadiabatic Quantum Dynamics. *Phys. Rev. A: At., Mol., Opt. Phys.* **1999**, *59*, 64−79.

DOI: 10.1021/acs.jctc.7b01178
J. Chem. Theory Comput. 2018, 14, 1828−1840

(58) Huo, P.; Coker, D. F. Semi-Classical Path Integral Non-Adiabatic Dynamics: A Partial Linearized Classical Mapping Hamiltonian Approach. *Mol. Phys.* **2012**, *110*, 1035−1052.
(59) Miller, W. H. The Semiclassical Initial Value Representation: A Potentially Practical way for Adding Quantum Effects to Classical molecular dynamics simulations. *J. Phys. Chem. A* **2001**, *105*, 2942−2955.
(60) Miller, W. H. Electronically Nonadiabatic Dynamics via Semiclassical Initial Value Methods. *J. Phys. Chem. A* **2009**, *113*, 1405−1415.
(61) Huo, P.; Miller, T. F., III; Coker, D. F. Communication: Predictive Partial Linearized Path Integral Simulation of Condensed Phase Electron Transfer Dynamics. *J. Chem. Phys.* **2013**, *139*, 151103.
(62) Huo, P.; Miller, T. F., III Electronic coherence and the kinetics of inter-complex energy transfer in light-harvesting systems. *Phys. Chem. Chem. Phys.* **2015**, *17*, 30914−30924.
(63) Castellanos, M. A.; Huo, P. Enhancing Singlet Fission Dynamics by Suppressing Destructive Interference between Charge-Transfer Pathways. *J. Phys. Chem. Lett.* **2017**, *8*, 2480−2488.
(64) Provazza, J.; Segatta, F.; Garavelli, M.; Coker, D. F. Semiclassical Path Integral Calculation of Nonlinear Optical Spectroscopy. *J. Chem. Theory Comput.* **2018**, *14*, 856.
(65) Bonella, S.; Coker, D. F. Semiclassical Implementation of the Mapping Hamiltonian Approach for Nonadiabatic Dynamics using Focused Initial Distribution Sampling. *J. Chem. Phys.* **2003**, *118*, 4370−4385.
(66) Darghouth, A.; Casida, M.; Taouali, W.; Alimi, K.; Ljungberg, M. P.; Koval, P.; Sánchez-Portal, D.; Foerster, D. Assessment of Density-Functional Tight-Binding Ionization Potentials and Electron Affinities of Molecules of Interest for Organic Solar Cells Against First-Principles GW Calculations. *Computation* **2015**, *3*, 616−656.
(67) Scholz, R.; Luschtinetz, R.; Seifert, G.; Jageler-Hoheisel, T.; Korner, C.; Leo, K.; Rapacioli, M. Quantifying charge transfer energies at donor-acceptor interfaces in small-molecule solar cells with constrained DFTB and spectroscopic methods. *J. Phys.: Condens. Matter* **2013**, *25*, 473201.
(68) Gaus, M.; Cui, Q.; Elstner, M. DFTB3: Extension of the Self-Consistent-Charge Density-Functional Tight-Binding Method (SCC-DFTB). *J. Chem. Theory Comput.* **2011**, *7*, 931−948.
(69) Gaus, M.; Goez, A.; Elstner, M. Parametrization and Benchmark of DFTB3 for Organic Molecules. *J. Chem. Theory Comput.* **2013**, *9*, 338−354.
(70) Aradi, B.; Hourahine, B.; Frauenheim, T. DFTB+, a Sparse Matrix-Based Implementation of the DFTB Method. *J. Phys. Chem. A* **2007**, *111*, 5678−5684.
(71) Rappe, A. K.; Casewit, C. J.; Colwell, K. S.; Goddard, W. A.; Skiff, W. M. UFF, a Full Periodic Table Force Field for Molecular Mechanics and Molecular Dynamics Simulations. *J. Am. Chem. Soc.* **1992**, *114*, 10024−10035.
(72) Abuabara, S. G.; Rego, L. G. C.; Batista, V. S. Influence of Thermal Fluctuations on Interfacial Electron Transfer in Functionalized TiO2 Semiconductors. *J. Am. Chem. Soc.* **2005**, *127*, 18234−18242.
(73) Pal, S.; Trivedi, D. J.; Akimov, A. V.; Aradi, B.; Frauenheim, T.; Prezhdo, O. V. Nonadiabatic Molecular Dynamics for Thousand Atom Systems: A Tight-Binding Approach Toward PYXAID. *J. Chem. Theory Comput.* **2016**, *12*, 1436−1448.
(74) Rego, L. G.; Hames, B. C.; Mazon, K. T.; Joswig, J.-O. Intramolecular Polarization Induces Electron-Hole Charge Separation in Light-Harvesting Molecular Triads. *J. Phys. Chem. C* **2014**, *118*, 126−134.
(75) Torres, A.; Oliboni, R. S.; Rego, L. G. Vibronic and Coherent Effects on Interfacial Electron Transfer Dynamics. *J. Phys. Chem. Lett.* **2015**, *6*, 4927−4935.
(76) Li, L.; Kanai, Y. Excited Electron Dynamics at Semiconductor: Molecule Type-II Heterojunction Interface: First-Principles Dynamics Simulation. *J. Phys. Chem. Lett.* **2016**, *7*, 1495−1500.
(77) Löwdin, P.-O. Some Properties of Inner Projection. *Int. J. Quantum Chem.* **1970**, *5*, 231−23.
(78) Akimov, A. V. Nonadiabatic Molecular Dynamics with Tight-Binding Fragment Molecular Orbitals. *J. Chem. Theory Comput.* **2016**, *12*, 5719−5736.
(79) Akimov, A. V.; Prezhdo, O. V. The PYXAID Program for Non-Adiabatic Molecular Dynamics in Condensed Matter Systems. *J. Chem. Theory Comput.* **2013**, *9*, 4959−4972.
(80) Coronado, E. A.; Xing, J.; Miller, W. H. Ultrafast Non-Adiabatic Dynamics of Systems With Multiple Surface Crossings: A Test of the Meyer-Miller Hamiltonian with Semiclassical Initial Value Representation Methods. *Chem. Phys. Lett.* **2001**, *349*, 521−529.
(81) Duke, J. R.; Ananth, N. Simulating Excited State Dynamics in Systems with Multiple Avoided Crossings Using Mapping Variable Ring Polymer Molecular Dynamics. *J. Phys. Chem. Lett.* **2015**, *6*, 4219−4223.
(82) Müller, U.; Stock, G. Flow of zero-point energy and exploration of phase space in classical simulations of quantum relaxation dynamics. II. Application to nonadiabatic processes. *J. Chem. Phys.* **1999**, *111*, 77−88.
(83) Stock, G. A Semiclassical Self-Consistent-Field Approach to Dissipative Dynamics. II. Internal Conversion Processes. *J. Chem. Phys.* **1995**, *103*, 2888−2902.
(84) Stock, G.; Thoss, M. Mixed Quantum-Classical Description of the Dynamics at Conical Intersection, Conical Intersections. In. *Conical Intersections*; Advanced Series in Physical Chemistry Series; Domcke, W., Yarkony, D. R., Köppel, H., Eds.; World Scientific: Singapore, 2004; pp 619−695.
(85) Walters, P. L.; Makri, N. Iterative Quantum-Classical Path Integral with Dynamically Consistent State Hopping. *J. Chem. Phys.* **2016**, *144*, 044108.
(86) Makarov, D. E.; Makri, N. Path Integrals for Dissipative Systems by Tensor Multiplication. Condensed Phase Quantum Dynamics for Arbitrarily Long Time. *Chem. Phys. Lett.* **1994**, *221*, 482−491.
(87) Ishizaki, A.; Fleming, G. R. Theoretical Examination of Quantum Coherence in a Photosynthetic System at Physiological Temperature. *Proc. Natl. Acad. Sci. U. S. A.* **2009**, *106*, 17255−17260.
(88) Zhu, J.; Kais, S.; Rebentrost, P.; Aspuru-Guzik, A. Modified Scaled Hierarchical Equation of Motion Approach for the Study of Quantum Coherence in Photosynthetic Complexes. *J. Phys. Chem. B* **2011**, *115*, 1531−1537.
(89) Jailaubekov, A. E.; Willard, A. P.; Tritsch, J. R.; Chan, W.-L.; Sai, N.; Gearba, R.; Kaake, L. G.; Williams, K. J.; Leung, K.; Rossky, P. J.; Zhu, X.-Y. Hot Charge-Transfer Excitons Set the Time Limit for Charge Separation at Donor/Acceptor Interfaces in Organic Photovoltaics. *Nat. Mater.* **2013**, *12*, 66−73.
(90) Lee, M.; Geva, E.; Dunietz, B. Donor-to-Donor vs. Donor-to-Acceptor Interfacial Charge Transfer States in the Phthalocyanine-Fullerene Organic Photovoltaic System. *J. Phys. Chem. Lett.* **2014**, *5*, 3810−3816.
(91) Hu, C.; Sugino, O.; Hirai, H.; Tateyama, Y. Nonadiabatic couplings from the Kohn-Sham derivative matrix: Formulation by time-dependent density-functional theory and evaluation in the pseudopotential framework. *Phys. Rev. A: At., Mol., Opt. Phys.* **2010**, *82*, 062508.

DOI: 10.1021/acs.jctc.7b01178
J. Chem. Theory Comput. 2018, 14, 1828−1840